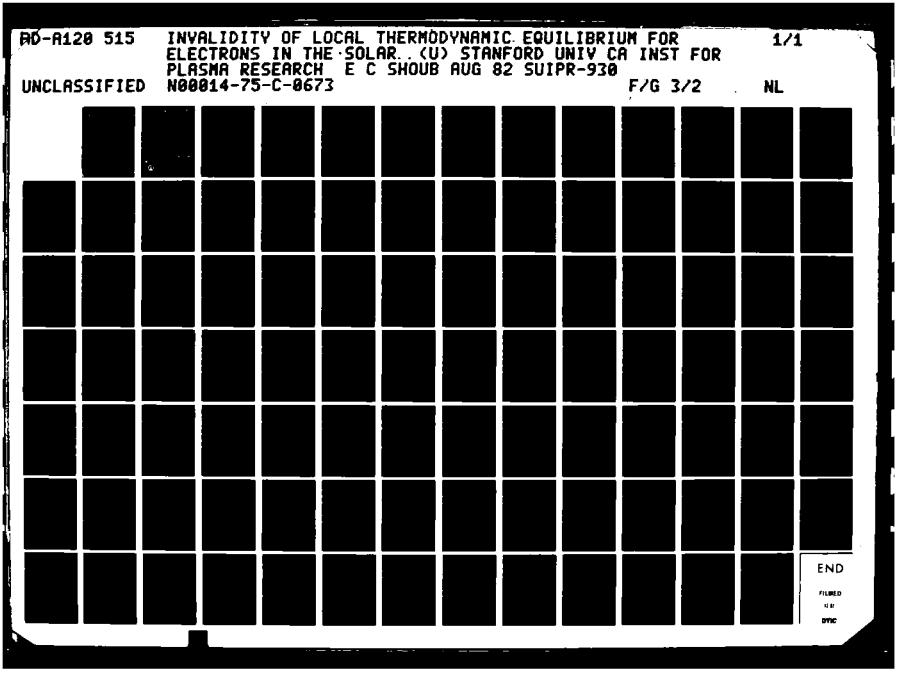
AD-A120 515
INVALIDITY OF LOCAL THERMODYNAMIC EQUILIBRIUM FOR ELECTRONS IN THE SOLAR.. (U) STANFORD UNIV CA INST FOR PLASMA RESEARCH E C SHOUB AUG 82 SUIPR-930
1/1
UNCLASSIFIED
N00014-75-C-0673
F/G 3/2
NL
END
FILMED
DTIC

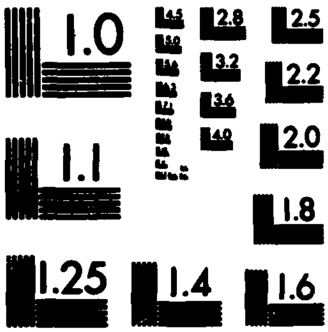

MICROCOPY RESOLUTION TEST CHART
NATIONAL BUREAU OF STANDARDS-1963-A

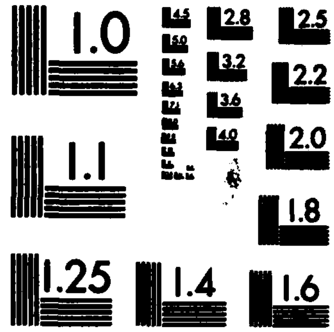

MICROCOPY RESOLUTION TEST CHART
NATIONAL BUREAU OF STANDARDS-1963-A

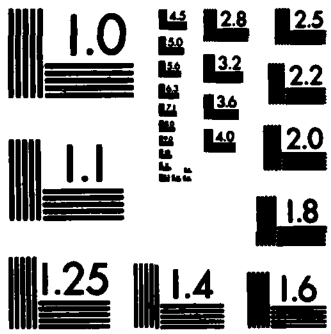

MICROCOPY RESOLUTION TEST CHART
NATIONAL BUREAU OF STANDARDS-1963-A

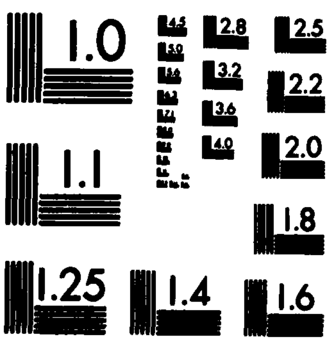

MICROCOPY RESOLUTION TEST CHART
NATIONAL BUREAU OF STANDARDS-1963-A

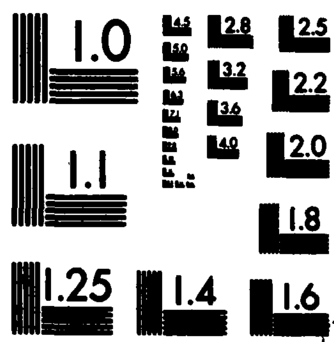

MICROCOPY RESOLUTION TEST CHART
NATIONAL BUREAU OF STANDARDS-1963-A

AD A120515

DTIC FILE COPY

LEVEL II

(6)

INVALIDITY OF LOCAL THERMODYNAMIC EQUILIBRIUM FOR ELECTRONS IN THE SOLAR TRANSITION REGION. I. FOKKER-PLANCK RESULTS

by

Edward C. Shoub

NATIONAL AERONAUTICS AND SPACE ADMINISTRATION
Grant NGL 05-020-272
Grant NAGW-92

OFFICE OF NAVAL RESEARCH
Contract N00014-75-C-0673

SUIPR Report No. 930

DTIC
ELECTE
OCT 19 1982
S D
E

August 1982

This document has been approved for public release and sale; its distribution is unlimited.

INSTITUTE FOR PLASMA RESEARCH
STANFORD UNIVERSITY, STANFORD, CALIFORNIA

82 09 28 026

Invalidity of Local Thermodynamic Equilibrium for Electrons in the Solar Transition Region. I. Fokker-Planck Results

Edward C. Shoub

Institute for Plasma Research

Stanford University

Stanford, California 94305

DTIC COPY INSPECTED 2

Accession For	
NTIS GRA&I	☑
DTIC TAB	☐
Unannounced	☐
Justification	
By Letter on file	
Distribution/	
Availability Codes	
Dist	Avail and/or Special
A	

Submitted to The Astrophysical Journal

August 1982

Abstract

An effective numerical method for solving boundary value problems for the Landau Fokker-Planck equation is developed and applied to calculating the electron velocity distribution function in model solar transition regions. Numerical results illustrating the speed, pitch angle and spatial dependence of the distribution function are presented. From these it is concluded that the widely-invoked assumption that in weakly inhomogeneous collisional plasma the angle-averaged distribution function remains close to local-Maxwellian distribution is incorrect. Instead, the distribution function forms an anisotropic, high velocity tail in the lower temperature regions due to the diffusion of fast electrons anti-parallel to the temperature gradient. Roughly speaking this effect is of quantitative signficance for spectroscopic work and heat conduction provided $\lambda \left(\frac{d\ell nT}{dz}\right)_{max} \gtrsim 10^{-3}$, where $\lambda = (kT)^2/\pi e^4 n \ell n \Lambda$ is an effective mean free path for thermal electrons.

It is shown that as a result of there being an excess of fast electrons in the low transition region ($T \lesssim 3 \times 10^5$ K, say), inelastic electron-ion collision rates are significantly enhanced over the Maxwellian values. Attendant effects on the ionization balance of a typical metal (magnesium) are shown to be significant. Implications of the breakdown of the local-Maxwellian approximation for several outstanding questions related to the solar transition region are discussed, including: energy balance in low transition region and upper chromosphere, the helium resonance line spectrum, the Schmahl-Orrall observation of continuum absorption by neutral hydrogen, and the origin of the 20,000 K temperature plateau.

Subject headings: plasmas - Sun: atmosphere - Sun: chromosphere - atomic processes.

I. Introduction

This is the first in a projected series of papers on the topic of how gradient in density and temperature affect the electron velocity distribution function (EVDF) in collisional plasma. For reasons to be discussed, emphasis throughout the series will be placed on physical conditions thought to exist in the Sun's chromosphere-corona transition region and upper chromosphere (hereafter referred to simply as the transition region; TR) and on assessing any implications of the kinetic theory to be developed for the spectroscopic diagnosis and energy balance of these regions. Results of more general interest will also be presented, however.

Knowledge of the form assumed by the EVDF in a plasma under weakly inhomogeneous conditions - those in which the effective mean free path of thermal electrons λ ($\lambda = (kT)^2 / \pi e^4 n \ln\Lambda$ in fully ionized hydrogen; see below) is everywhere small relative to gradient scale lengths - is an essential element in many astrophysical analyses. Such knowledge is required, for example, in order to determine electron-ion collisional excitation and ionization rates and the plasma thermal and electrical conductivities.

Although the Sun's TR is known from EUV observations to be the site of unusually large temperature and density gradients, it nonetheless qualifies as a weakly inhomogeneous medium under the definition given above. This point is illustrated by Table 1 showing portion of an empirically derived, spatially averaged, quiet-sun TR model published by Dupree (1972.) Note that $\alpha \equiv \lambda \frac{d\ln T}{dz} \lesssim 5 \times 10^{-2}$. Consequently, it is generally thought that throughout the Sun's TR, as in any quasi-stationary, weakly inhomogeneous plasma, the EVDF can be adequately approximated by an expression of the form

$$f(\underset{\sim}{r}, v, z) = f^*(v; n, T)\left\{1 + \alpha(z) D\left(\frac{v}{v_{th}}\right) + O(\alpha^2)\right\}, \qquad (1)$$

where I have considered the simplest case of a horizontally stratified ($\nabla T = \frac{dT}{dz}\hat{e}_z$), isobaric plasma at rest with a vertical (or zero) magnetic field. Here f* is a local-Maxwellian distribution with number density n and temperature T, $\mu = \frac{\underline{v}.\hat{e}_z}{|\underline{v}|}$, and D (x) is obtained by applying the Chapman-Enskog formalism to a particular kinetic equation, as done, for example, by Spitzer and Härm (1953) for the Fokker-Planck equation.

Equation (1) has two important implications: first the angle-averaged distribution $f^o = \frac{1}{2}\int_{-1}^{1} f d\mu$, remains equal to a local Maxwellian distribution, and second, the electron heat flux, $q \equiv 2\pi \frac{m}{2}\int_{-1}^{1}\mu d\mu \int_0^\infty v^5 f(\mu, v, z)\, dv$, is proportional to $T^{5/2}\frac{dT}{dz}$ and is only logarithmically dependent on density. These conclusions underlie many solar and astrophysical analyses, including ionization equilibrium and radiative loss calculations, spectroscopic diagnostic procedures and energy balance arguments. It is my aim in this and later papers in this series to show that they are, in fact, invalid in the solar transition region - and, by implication, under similar conditions in other inhomogeneous media.

The difficulty is that equation (1) is not a uniformly valid approximation (Shoub 1976, 1981); it fails for electron velocities $v \gtrsim v_c$, where v_c is defined by the relation $\alpha \left(\frac{v_c}{v_{th}}\right)^4 = 1$. The reason for this failure is that according to Landau's (1936; 1949) Fokker-Planck equation (the same equation was later derived using different arguments by Spitzer and Härm (1953) and later still by Rosenbluth, MacDonald and Judd; RMJ 1957), the effective speed-dependent mean free path of an electron in a fully ionized gas increases as the fourth power of its velocity, for velocities greater than thermal. As defined above, v_c is the

velocity at which an electron's mfp equals the local temperature-gradient scale length. The ratio v_c/v_{th} is listed in Table 1; note that it falls well-within the range relevant to calculating inelastic collision rates. Equation (1) fails for $v>v_c$ because its derivation is based on the assumed existence of "normal", or, in present context, spatially local solutions to a kinetic equation of the form

$$f(\underline{v}, z) = f(\underline{v}; n(z), T(z), \nabla n(z), \nabla T, \ldots)$$

where the ellipsis denotes higher order gradients. It seems clear, at least intuitively, that such a local solution cannot exist at velocities for which electrons can traverse one or more scale heights before thermalizing. This can be seen from a mathematical standpoint as follows.

Consider the dimensionless, high-velocity form of the RMJ Fokker-Planck equation in the Maxwellian-field-particle approximation (hereafter MFPA), namely

$$\mu\xi^4 \left\{\frac{\partial\phi}{\partial\tau} - \frac{\alpha(\tau)}{2}\left(\xi\frac{\partial\phi}{\partial\xi} + 5\phi\right)\right\} = \frac{1}{2}\frac{\partial^2\phi}{\partial\xi^2} + \left(\xi - \frac{1}{2\xi}\right)\frac{\partial\phi}{\partial\xi} + \frac{\partial}{\partial\mu}\left\{(1-\mu^2)\frac{\partial\phi}{\partial\mu}\right\} \qquad (2)$$

where

$$\phi = \frac{2\pi v_{th}^3}{n_o} f;\ \xi = \frac{v}{v_{th}};\ v_{th}^2(z) = \frac{2kT_o(z)}{m};\ \mu = \frac{\underline{v}}{|\underline{v}|}\cdot\hat{e}_z$$

$$\tau = \int_o^z \frac{dz'}{\lambda(z')};\ \lambda(z) = \frac{\left(k\,T_o(z)\right)^2}{\pi e^4 n_o(z)\ell n\Lambda}$$

$$\alpha = \lambda\frac{d\ell n(T_o)}{dz} = \frac{d\ell n(T_o)}{d\tau}$$

Equation (2) follows from the full Fokker-Planck equation upon evaluating the Rosenbluth potentials (see Eqn. 9) using a local-Maxwellian distribution for electrons, a delta function distribution at zero velocity for protons and then neglecting terms in the resulting coefficients which are unimportant

at large velocities. A thermal electric field term has also been omitted from the left side of (2); it is unimportant relative to gradient-related terms at large velocities (see Eqn. 41). The quantities T_o and n_o are reference variables which for the moment may be identified with the electron temperature and density. Note that λ, referred to above as the effective mean free path of thermal electrons, is simply the length scale which emerges from non-dimensionalizing the Fokker-Planck equation. Its numerical value depends on the choice of characteristic velocity v_{th}; the invariant quantity is $\lambda\left(\frac{v}{v_{th}}\right)^4$. The left side of Eqn. (2) is proportional to $\frac{df}{dz}$ and incorporates the relation $n_o T_o$ = constant. The ξ-derivative terms on the right derive from electron-electron collisions while the μ-derivative term contains equal contributions from electron-electron and electron-proton scattering. A factor of ξ^3 has been brought to the left side in (2) to facilitate the following argument. Note, finally, that disregarding boundary conditions, a local-Maxwellian $\phi^* = \frac{2}{\sqrt{\pi}}e^{-\xi^2}$, satisfies Eqn. (2) when $\alpha(\tau) \equiv 0$. Eqn. (2) is derived in detail in §II.

Consider now the traditional (Chapman-Enskog) argument leading from Eqn. (2) to Eqn. (1). First, one seeks a spatially-local (normal) solution of (2) in which there is no explicit spatial variation of ϕ, but only an implicit one arising from its dependence on the thermodynamic variables and their gradients. In the context of Eqn. (2) this means we look for solutions of the form $\phi\ (\mu, \xi, \tau;\ \alpha(\tau)) = \phi(\mu, \xi; \alpha, \frac{\partial\alpha}{\partial\tau}, \ldots)$. Second, since α is presumed small, one <u>assumes</u> that ϕ may be expanded as a power series in the α. (This is known in the kinetic theory literature as the Hilbert expansion assumption; see, e.g., Résibos and De Leener 1977).

Thus

$$\phi \simeq \phi^0(\mu, \xi) + \alpha\phi^1(\mu, \xi) + \ldots .$$

On substituting this expansion into (2) and noting that $\frac{\partial\phi}{\partial\tau} = \frac{\partial\phi}{\partial\alpha}\frac{\partial\alpha}{d\tau} = 0\ (\alpha^2)$, one finds, in the usual way, that

$$\phi(\mu, \xi, \tau) = \phi^*(\xi)\{1 + \mu\alpha\ \phi^1(\xi) + 0\ (\alpha^2)\},$$

where ϕ^* is a local-Maxwellian and ϕ^1 satisfies an inhomogeneous ordinary differential equation. This procedure, then, is, in essence, the origin of the well-known Spitzer-Härm (1953) solution. It is seen that the approximation of local thermodynamic equilibrium (LTE) - taken here to mean that $\frac{1}{2}\int_{-1}^{1} \phi\ d\mu \simeq \phi^*$ - is a necessary consequence of the assumption that the distribution function may be expanded in a power series in the gradients, for a local-Maxwellian must be annihilated by any viable collision integral. LTE is therefore built into, rather than deduced from, the Chapman-Enskog analysis.

But inspection of Eqn. (2) clearly shows that the regular-perturbative approach just described cannot give valid results at velocities for which $\alpha\xi^4 \geq 0\ (1)$. In this regime the gradient-related terms in (2) dominate the collision terms, and this precludes finding meaningful spatially-local solutions.

The actual form assumed by the tail of the EVDF under conditions for which $\alpha\xi^4$ becomes of order unity at moderate velocities is thus an open question - and is the question addressed in this paper. The approach taken has been to mount a careful numerical attack on the RMJ Fokker-Planck equation - in the present context a quasi-linear, second-order, partial differential equation in three independent variables with half-range boundary conditions. The numerical method developed is a fourth-order, fully implicit, finite difference algorithm. After extensive testing, the code was applied

to calculating the EVDF for the simplest relevant models of the solar TR, namely inhomogeneous plasma slabs of fully ionized hydrogen with a vertical (or zero) magnetic field. (Optically thin radiation is alsc allowed for, but not self-consistently.) Inhomogenity is introduced via boundary conditions on the incoming distribution functions. The main conclusion drawn from these calculations is that the local-Maxwellian approximation is badly in error throughout the middle and lower TR. The computed distributions exhibit a pronounced, anisotropic, high-velocity tail attributable to the free streaming of fast electrons from hotter overlying layers. This effect causes collisional ionization rates (and in some cases excitation rates) to be enhanced over their LTE-values, often by several orders of magnitude.

The numerical results reported here have been obtained in the Maxwellian-field-particle-approximation (MFPA), meaning that the Rosenbluth potentials which enter the Fokker-Planck equation are evaluated using a local-Maxwellian distribution for electrons. In §III I show that although this approximation gives the angle-averaged part of the distribution function accurately, its use, together with my not having calculated the distribution function out to sufficiently large velocities, precludes an accurate determination of the electron flux. The heat flux question is therefore deferred to a later publication.

The rest of the paper is organized as follows: In §II I present the mathematical model and discuss its limitations. In §III I discuss the numerical algorithm and, in §IV, give detailed results for the distribution function, showing its spatial, velocity and pitch angle dependence. In this section I also calculate inelastic collisi:n rates for helium and magnesium and show how the enhanced ionization rates alter magnesium's ionization equilibrium. In §V I discuss possible implications of the results and

suggest that several observational and theoretical puzzles concerning the low TR and upper chromosphere might be resolved by consideration of this effect. The paper ends with a critical review of the recent literature on this topic (Spicer [1979], Roussel-Dupré [1980a,b], Gurevich and Istomin [1979]) and a summary of results.

II. Model Definition

I consider an idealized TR consisting in a constant pressure slab of fully ionized hydrogen containing a fictitious trace ion in sufficient amount to allow the plasma to radiate energy at a rate equal to that radiated by an optically thin plasma with cosmic element abundances, as calculated by McWhirter et al. (1975). The slab has thickness L and any magnetic field present is assumed to lie along the gradient direction. The protons are taken to be infinitely massive, at rest, and distributed so as to provide charge neutrality. I neglect the trace ion's contribution to the charge balance so that $n_p = n_e \equiv n$. The constraint that no steady current flow through the TR then implies that the average electron velocity must be zero. Inhomogenity is introduced via boundary conditions on the incoming electron distribution function on the planes $z = 0$ and $z = L$, as described below. Finally, I assume that the EVDF obeys the Fokker-Planck equation, in the form derived by Rosenbluth, MacDonald and Judd (1957). Several limitations of this central assumption should be mentioned.

First, the RMJ equation is, at best, accurate only to within terms of order $(\ln \Lambda)^{-1}$; i.e., to "dominant order" (e.g., Grad 1962). Moreover, it appears (Spitzer 1962, Siambis and Stitzer[1] 1974) that the "dominant" approximation is not uniformly valid in velocity. More specifically, a non-dominant contribution to the parallel $(\hat{e}_v \hat{e}_v)$ component of the velocity diffusion tensor, which of course is omitted from the RMJ equation, decays

---

1 Siambis and Stitzer erroneously attribute differences between their results for the parallel diffusion coefficient and those of Spitzer (1962) (and RMJ) to their retention of a velocity-dependent Coulomb logarithm. The latter refinement leads only to minor corrections to the Spitzer result however. The main reason for the discrepancy lies in their keeping a non-dominant term which is neglected by Spitzer.

as v^{-1} for large v, whereas the dominant contribution decays as v^{-3}. The neglected term is therefore no longer negligible for $\left(\frac{v}{v_{th}}\right)^2 \gtrsim 0\ (\ell n\ \Lambda)$. Nevertheless, Siambis and Stitzer show that the contribution of the neglected term to the energy loss rate of a test particle is of relative order $(\ell n\ \Lambda)^{-1}$ at all velocities, thereby leading one to suspect that its retention would not significantly alter results obtained from the RMJ equation. This latter conjecture is currently under investigation.

Second, because the RMJ equation was derived from consideration of successive but uncorrelated binary events, its use precludes consideration of possible collective effects. However, in the present problem, where the question is whether significant departures from a local-Maxwellian distribution exist under conditions in which classical theory suggests they do not, the disregard of collective effects may be viewed as a plausible working hypothesis, which may be checked a posteriori, at least in principle. In practice, furnishing proof that collective effects are unimportant is likely to be difficult. Not only must one demonstrate stability against both electrostatic and electromagnetic perturbations, but one must also show that electron scattering by enhanced plasma fluctuations, which arise even in stable non-Maxwellian plasmas (e.g., Tidman and Eviatar 1965), is negligible compared to Coulomb scattering. Clearly, then, the question of collective effects in the present context is an involved one, and is likely to be a fruitful area of future research. It is not addressed further in this paper. The reader should bear in mind that such effects may alter conclusions drawn below.

Third, and lastly, note that because the effect of a background magnetic field on binary collision dynamics is ignored in the RMJ equation, its use is limited to situations in which the mean electron gyroradius

is large compared with the Debye length (e.g., Baldwin and Watson 1975). This requires $B \lesssim 10^{-2} n^{1/2}$, where B is the magnetic field strength in gauss and n is the electron density in cm^{-3}. This condition is not overly restrictive for solar applications.

Consider now the appropriateness of a time-independent calculation. For a TR with nT = const. = 6×10^{-14} K cm^{-3}, the electron-electron relaxation time, $\nu_{ee}^{-1}(v) = \frac{\lambda}{v_{th}} \left(\frac{v}{v_{th}}\right)^3 \approx 3.5 \times 10^{-16} \frac{T^{5/2}}{\ell n\, \Lambda} \left(\frac{v}{v_{th}}\right)^3$, varies between $5 \times 10^{-3} \left(\frac{v}{v_{th}}\right)^3$ sec at the top of the TR ($T = 10^{5.8}$ K, $\ell n\, \Lambda = 20$) and $3 \times 10^{-7} \left(\frac{v}{v_{th}}\right)^3$ sec at the bottom ($T = 10^4$ K, $\ell n\, \Lambda = 11$). Thus, even in the far tail of the distribution $\left(\frac{v}{v_{th}} \sim 5\right)$, stationarity is achieved in approximately one second at the top of the TR and in 10^{-4} sec at the bottom. On the other hand, relevant macroscopic time scales, for example, the rise times of spicules, are typically of the order of minutes (e.g., Athay 1976, p. 114).

Proceeding, I write the electron Fokker-Planck equation as

$$\underline{v} \cdot \frac{\partial f}{\partial \underline{x}} - \frac{e}{m} \left(\underline{E} + \frac{\underline{v}}{c} \times \underline{B}\right) \cdot \frac{\partial f}{\partial \underline{v}} = \left.\frac{\delta f}{\delta t}\right|_{e\ell} + \left.\frac{\delta f}{\delta t}\right|_{inel.} \qquad (3)$$

Here -e and m are the electron charge and mass, $\underline{E}$ is the self-consistent polarization electric field required for zero current flow, and the terms on the right represent elastic and inelastic collision terms. The latter are included to allow for the effect of radiative losses on the electron temperature. The distribution function f is normalized to the average electron number density.

Let $(\hat{e}_x, \hat{e}_y, \hat{e}_z)$ be an orthonormal triplet with $\hat{e}_z$ in the direction of increasing temperature. I adopt a spherical coordinate system in velocity space (v, θ, β) with polar axis along $\hat{e}_z$. The corresponding unit vectors are

$$\hat{e}_v = \cos\theta\ \hat{e}_z + \sin\theta\ (\cos\beta\ \hat{e}_x + \sin\beta\ \hat{e}_y) \tag{4a}$$

$$\hat{e}_\theta = -\sin\theta\ \hat{e}_z + \cos\theta\ (\cos\beta\ \hat{e}_x + \sin\beta\ \hat{e}_y) \tag{4b}$$

$$\hat{e}_\beta = -\sin\beta\ \hat{e}_x + \cos\beta\ \hat{e}_y \tag{4c}$$

It will be useful below to note that

$$\nabla_{\underline{v}} = \hat{e}_v \frac{\partial}{\partial v} + \hat{e}_\theta \frac{1}{v}\frac{\partial}{\partial\theta} + \frac{\hat{e}_\beta}{v\sin\theta}\frac{\partial}{\partial\beta} \tag{5a}$$

and that

$$\frac{\partial e_v}{\partial\theta} = \hat{e}_\theta\ ;\ \frac{\partial\hat{e}_\theta}{\partial\theta} = -\hat{e}_v \tag{5b}$$

$$\frac{\partial\hat{e}_v}{\partial\beta} = \sin\theta\ \hat{e}_\beta\ ;\ \frac{\partial\hat{e}_\theta}{\partial\beta} = \cos\theta\ \hat{e}_\beta\ ;\ \frac{\partial\hat{e}_\beta}{\partial\beta} = -(\sin\theta\ \hat{e}_v + \cos\theta\ \hat{e}_\theta)$$

with all other unit-vector derivatives equal to zero.

Now consider the magnetic field terms in (3). With $\underline{B} = B\ \hat{e}_z$ I find that

$$-\frac{e}{mc}(\underline{v}\times\underline{B})\cdot\frac{\partial f}{\partial\underline{v}} = \Omega\frac{\partial f}{\partial\beta}\ , \tag{6}$$

where $\Omega = eB/mc$ is the electron gyrofrequency. The spatial gradient term in (3) is

$$\underline{v}\cdot\frac{\partial f}{\partial x} \equiv v\cos\theta\frac{\partial f}{\partial z} + \sin\theta\left(\cos\beta\frac{\partial f}{\partial x} + \sin\beta\frac{\partial f}{\partial y}\right), \tag{7}$$

$$= v\cos\theta\frac{\partial f}{\partial z}\ ,$$

where the second equality follows from the assumed homogeneity of f in the x-y plane. If, in the boundary conditions,

$$f(\underline{v},\ z = 0) = f_b^+(\underline{v})\ ;\ \underline{v}\cdot\hat{e}_z > 0$$

$$f(\underline{v},\ z = L) = f_b^-(\underline{v})\ ;\ \underline{v}\cdot\hat{e}_z < 0, \tag{8}$$

the prescribed functions $f_b^{\pm}$ are chosen β-independent, it then follows that $\frac{\partial f}{\partial \beta} \equiv 0$, for there are no further terms in (3) which introduce a β-dependence into f. Thus, under the above restrictions the magnetic field has no effect on the distribution function. Viewed differently, a vertical magnetic field is irrelevant because, for a given pitch angle, the helical and slant pathlength between heights z_1 and z_2 are equal.

Following Rosenbluth et al. (1957) I write

$$\left.\frac{\delta f}{\delta t}\right|_{e\ell} = \sum_\alpha \Gamma_{e\alpha}\left\{-\frac{\partial}{\partial \underline{v}}\cdot\left(\frac{\partial h_\alpha}{\partial \underline{v}}\, f\right) + \frac{1}{2}\frac{\partial^2}{\partial \underline{v}\partial \underline{v}} : \left(\frac{\partial^2 g_\alpha}{\partial \underline{v}\partial \underline{v}}\, f\right)\right\} \tag{9a}$$

$$\Gamma_{e\alpha} = \frac{4\pi e^4 Z_\alpha^2}{m^2}\ \ell n\ \Lambda \tag{9b}$$

$$h_\alpha(z,\underline{v}) = \left(\frac{m + m_\alpha}{m_\alpha}\right)\int \frac{f_\alpha(z,\underline{v}')}{|\underline{v} - \underline{v}'|}\, d^3\underline{v}' \tag{9c}$$

$$g_\alpha(z,\underline{v}) = \int f_\alpha(z,\underline{v}')\ |\underline{v} - \underline{v}'|\ d^3\underline{v}' \tag{9d}$$

Here unsubscripted species-dependent quantities refer to electrons and the summation in (9a) is over electrons and protons. It follows from (9c, d) that

$$\nabla_{\underline{v}}^2 g_\alpha = \frac{2m_\alpha}{m+m_\alpha} h_\alpha, \text{ and from the relation } \nabla_{\underline{v}}^2 |\underline{v} - \underline{v}'|^{-1} = -4\pi\delta^3(\underline{v} - \underline{v}')$$

that $\nabla_{\underline{v}}^2 h_\alpha = -4\pi \left(\frac{m + m_\alpha}{m_\alpha}\right) f_\alpha$. Use of these equations allows (9a) to be rewritten as

$$\left.\frac{\delta f}{\delta t}\right|_{e\ell} = \sum_\alpha \Gamma_{e\alpha} \left\{ \left(\frac{m_\alpha - m}{m_\alpha + m}\right) \frac{\partial h_\alpha}{\partial \underline{v}} \cdot \frac{\partial f}{\partial \underline{v}} + \frac{1}{2} \frac{\partial^2 g_\alpha}{\partial \underline{v}\partial \underline{v}} : \frac{\partial^2 f}{\partial \underline{v}\partial \underline{v}} + 4 \frac{m}{m_\alpha} f_\alpha f \right\}, \tag{10}$$

a form useful for computational work because the electron-electron potential h_e does not appear.

I next write the right side of (10) in coordinate form, beginning with the electron-proton terms. Under the stated idealizations $f_p = n\,\delta^3(\underline{v})$, so that (9c) implies $h_p = \left(1 + \frac{m}{m_p}\right) \frac{n}{v} \approx \frac{n}{v}$, and (9d) implies $g_p = nv$. Using (5) and (6) I now find that

$$\frac{\partial h_p}{\partial \underline{v}} = -\frac{n}{v^2} \hat{e}_v \tag{11a}$$

$$\frac{\partial^2 g_p}{\partial \underline{v}\partial \underline{v}} = \frac{n}{v} (\hat{e}_\theta \hat{e}_\theta + \hat{e}_\beta \hat{e}_\beta). \tag{11b}$$

With $f = f(z, \theta, v)$ I also find that

$$\frac{\partial f}{\partial \underline{v}} = \hat{e}_v \frac{\partial f}{\partial v} + \frac{\hat{e}_\theta}{v} \frac{\partial f}{\partial \theta} \tag{12a}$$

$$\frac{\partial^2 f}{\partial \underline{v}\partial \underline{v}} = \hat{e}_v \hat{e}_v \frac{\partial^2 f}{\partial v^2} + \hat{e}_\theta \hat{e}_\theta \left(\frac{1}{v^2} \frac{\partial^2 f}{\partial \theta^2} + \frac{1}{v} \frac{\partial f}{\partial v}\right) \tag{12b}$$

$$+ \hat{e}_\beta \hat{e}_\beta \left(\frac{1}{v} \frac{\partial f}{\partial v} + \frac{\cot\theta}{v^2} \frac{\partial f}{\partial \theta}\right) + \left(\frac{\hat{e}_v \hat{e}_\theta + \hat{e}_\theta \hat{e}_v}{v}\right)\left(\frac{\partial^2 f}{\partial \theta \partial v} - \frac{1}{v} \frac{\partial f}{\partial \theta}\right)$$

with similar expressions for $\frac{\partial g_e}{\partial \underline{v}}$ and $\frac{\partial^2 g_e}{\partial \underline{v}\partial \underline{v}}$.

It remains only to perform the contractions indicated in (10). Neglecting the term $4\pi \frac{m}{m_p} f_p f$ and changing variables from θ to $\mu = \cos\theta$, I find the electron proton-scattering term to be

$$\left\{ \frac{\partial h_p}{\partial \underline{v}} \cdot \frac{\partial f}{\partial \underline{v}} + \frac{1}{2} \frac{\partial^2 g_p}{\partial \underline{v}\partial \underline{v}} : \frac{\partial^2 f}{\partial \underline{v}\partial \underline{v}} \right\} = \frac{n}{2v^3} \frac{\partial}{\partial \mu} \left\{ (1 - \mu^2) \frac{\partial f}{\partial \mu} \right\} \tag{13}$$

For the electron-electron terms I obtain

$$\left\{ \frac{1}{2} \frac{\partial^2 g_e}{\partial \underline{v}\partial \underline{v}} : \frac{\partial f}{\partial \underline{v}\partial \underline{v}} + 4\pi f^2 \right\} = a \frac{\partial^2 f}{\partial v^2} + b \frac{\partial^2 f}{\partial v \partial \mu} + c \frac{\partial^2 f}{\partial \mu^2} + d \frac{\partial f}{\partial v} + e \frac{\partial f}{\partial \mu} + pf, \tag{14}$$

where

$$a = \frac{1}{2} \frac{\partial^2 g}{\partial v^2} \tag{15a}$$

$$b = \frac{1 - \mu^2}{v^2} \left\{ \frac{\partial^2 g}{\partial \mu \partial v} - \frac{1}{v} \frac{\partial g}{\partial \mu} \right\} \tag{15b}$$

$$c = \frac{1 - \mu^2}{2v^3} \left\{ \frac{\partial g}{\partial v} + \frac{1}{v} \left[(1 - \mu^2) \frac{\partial^2 g}{\partial \mu^2} - \mu \frac{\partial g}{\partial \mu} \right] \right\} \tag{15c}$$

$$d = \frac{1}{v^2} \frac{\partial g}{\partial v} + \frac{1}{2v^3} \frac{\partial}{\partial \mu} \left[(1 - \mu^2) \frac{\partial g}{\partial \mu} \right] \tag{15d}$$

$$e = \frac{1}{v^3} \left\{ \frac{1}{v} \frac{\partial g}{\partial \mu} - \mu \frac{\partial g}{\partial v} - (1 - \mu^2) \left[\frac{\partial^2 g}{\partial \mu \partial v} + \frac{\mu}{2v} \frac{\partial^2 g}{\partial \mu^2} \right] \right\} \tag{15e}$$

$$p = 4\pi f \tag{15f}$$

For notational convenience I have dropped the subscript from g_e in (15a - e).

Now consider the inelastic collision term in (2). Let the imaginary trace element have two bound levels with energy difference E_{12} and number densities N_1, N_2 and let $\sigma_{12}(v)$ denote the inelastic cross section (assumed to be isotropic). For simplicity I take $N_2 = 0$, in which case (cf. Bernstein 1979, Shoub 1977)

$$\left.\frac{\delta f}{\delta t}\right|_{\text{inel.}} = N_1 \left\{ \frac{\bar{v}^2}{v}\, \sigma_{12}(\bar{v})\, \frac{1}{2} \int_{-1}^{1} d\mu'\, f(\mu', \bar{v}) - v\, \sigma_{12}(v)\, f(\mu, v) \right\} \qquad (16)$$

where, by virtue of energy conservation,

$$\frac{1}{2} m \bar{v}^2 = \frac{1}{2} m v^2 + E_{12}$$

It follows from (16) that the rate per unit volume at which energy is lost from electrons due to inelastic collisions is

$$-\int d^3 \underline{v} \left(\frac{1}{2} m v^2\right) \left.\frac{\delta f}{\delta t}\right|_{\text{inel.}} = 2\pi N_1 E_{12} \int_{v_{12}}^{\infty} dv\, v^3\, \sigma_{12}(v) \int_{-1}^{1} d\mu f(\mu, v)\,, \qquad (17)$$

where $v_{12} = \left(\frac{2 E_{12}}{m}\right)^{1/2}$. N_1 is determined by equating the right side of (17) to the rate per unit volume at which energy is radiated by the plasma.

As mentioned, I take the latter rate to be $n^2 \phi(T)$, where n is the electron density and $\phi(T)$ is the function given by McWhirter et al. (1975). I have arbitrarily chosen

$$\sigma_{12}(v) = \begin{cases} 0; & v \leq v_{12} \\ \pi a_o^2; & v > v_{12} \end{cases} \tag{18a}$$

where $a_o = 5.29 \times 10^{-9}$ cm, and we have let $E_{12} = E_{12}(z) = 4kT_o(z)$, where $T_o(z)$ is defined below. (18b)

Although the above treatment of the inelastic collision terms is schematic, it adequately accounts for the effect of radiative losses on the electron temperature profile. On the other hand, it is inadequate for treating possible distortion of the electron energy spectrum by imbalanced inelastic collisions, and it is therefore pertinent to ask if such distortion will occur in the low TR. The answer, most likely, is that it will not. Any tendency of imbalanced inelastic collisions to form bumps or dips will be overpowered by the smoothing, Maxwellian-producing action of electron-electron collisions, provided the collision frequency of the latter exceeds the inelastic collision frequency. For thermal hydrogen plasma this is the case provided $\frac{n_H}{n_e} \lesssim 10^2$ (Shoub 1977), where n_H is the neutral hydrogen density. In the upper chromosphere, $n_H < n_e$ ($n_H < 20\, n_e$ in the region where hydrogen Lyman-α formed), and electron-trace ion inelastic collision frequency is very small relative to the elastic collision frequency. Thus, except in the event that non-thermal enhancements of the hydrogen 1-2 excitation rate (§ IV) are as large as factors of 10^3 - 10^4, distortion of the electron energy spectrum by inelastic collisions is unlikely to be important.

Dimensionless Variables

In going from the chromosphere ($T \tilde{\sim} 10^4$K) to corona ($T = 2 \times 10^6$K) the electron thermal velocity increases by a factor of roughly 14. For computational purposes it is therefore convenient to work with dimensionless variables. Toward this end I introduce reference temperature, density and thermal velocity scales denoted $T_o(z)$, $n_o(z)$ and $v_{th}(z) = (2kT_o/m)^{1/2}$ respectively, and choose

$$n_o(z)\ T_o(z) = P = \text{constant}, \tag{19}$$

as is appropriate for isobaric slabs. In principle $T_o(z)$ may be any monotonic function satisfying $T_o(z = 0) = T_c$ and $T_o(z = L) = T_h$, where T_c and T_h are temperatures characterizing the incoming distribution functions at the boundaries. In practice it has been found most economical to have $T_o(z)$ conform as closely as possible to the actual temperature structure of the atmosphere. I therefore choose $T_o(z)$ as the solution of the macroscopic electron energy equation

$$\frac{d}{dz}\left(\frac{K}{\ell n\ \Lambda}\ T_o^{5/2}(z)\ \frac{dT_o}{dz}\right) + n_o^2\ \phi(T_o) = 0 \tag{20}$$

$$T_o(z = 0) = T_c$$

$$T_o(z = L) = T_H$$

Here $K = 1.87 \times 10^{-5}$ erg/ ($^oK^{7/2}$-cm-sec) is the constant in the Spitzer-Härm thermal conductivity, L is the slab thickness, $\Lambda = 3(kT_o)^2\ e^{-3}\ (4\pi P)^{-1/2}$, and $\phi(T_o)$ is McWhirter et al.'s heating function, modified to allow for the partial ionization of hydrogen as described in their paper. I represent ϕ analytically using a piecewise-linear fit ($\log \phi$ vs. $\log T_o$) to their graph. Equation (20) is solved numerically using finite differences in conjunction with generalized Newton-Raphson iteration.

I note that the $T_o(z)$ determined via (20) will differ from the T(z), the temperature determined from the Fokker-Planck equation, only to the extent that the true heat flux differs from that predicted by the Spitzer-Härm formula. Even the latter T(z) is not self-consistent however, due to the dependence of the radiative losses, which I am taking as given, on the tail of the electron distribution function. Except for a few brief remarks in §IV, I do not address this latter problem here.

Now consider my choices for the parameters L, T_c and T_h. Ideally one would locate the upper boundary at the point of maximum temperature in the corona (i.e., at $R \gtrsim 3\text{-}4\ R_\odot$), thereby accounting for the entire reservoir of hot plasma capable of supplying fast electrons to the underlying TR. And the lower boundary would ideally be located deep in chromosphere in order to insure that all electrons thermalize within the slab. Unfortunately, to model this expanse of atmosphere correctly requires consideration of several effects - pressure gradients, spherical geometry, self-consistent ionization equilibrium calculations for hydrogen and the other major electron donors - which were judged best omitted from this exploratory calculation. Thus I have chosen the thickest slab for which constant pressure remains a reasonable assumption ($L = 5 \times 10^4$ km), and a lower boundary temperature high enough that hydrogen remains almost fully ionized within the slab ($T_c = 8100$K). I set the upper boundary temperature T_h equal to the average coronal value of 2×10^6K. Numerical results are reported for these values of T_c, T_h and L, and for several pressures.

Returning to our discussion of the Fokker-Planck equation, I introduce the dimensionless variable:

$$\underline{\xi} = \underline{v}/v_{th} \tag{21a}$$

$$\tau = \int_0^z \frac{dz'}{\lambda(z')} \; ; \; \lambda = \frac{(k\, T_o(z))^2}{\pi e^4\, n_o\, \ell n\, \Lambda} \tag{21b}$$

$$\phi(\underline{\xi},\tau) = \frac{2\pi\, v_{th}^3}{n_o} f(\underline{v},\, z) \tag{21c}$$

$$\ell(\underline{\xi},\tau) = \frac{\ell\, g}{n_o v_{th}} = \frac{1}{2\pi} \int |\, \underline{\xi} - \underline{\xi}'\, |\, \phi(\underline{\xi}',\tau)\, d^3\underline{\xi}' \tag{21d}$$

and parameters

$$\alpha = \lambda \frac{d\ \ell n\ T_o}{dz} = \frac{d\ \ell n\ T_o}{d\tau} \tag{21e}$$

$$\beta = \frac{e\, E_z \lambda}{2\, kT_o} \tag{21f}$$

$$\eta = \frac{\pi\, a_o^2\, N_1/n_0}{\pi(e^2/kT_o)^2\, \ell n\, \Lambda} \tag{21g}$$

To facilitate comparisons, I note that $\alpha = \frac{1}{2} B_T$, $\beta = -\frac{1}{2} A_E = \frac{E_z}{E_c}$, where A_E and B_T are the parameters appearing in Spitzer and Härm's (1953) paper and E_c is Dreicer's (1959) critical field. The parameter η enters the FPE as a factor of the inelastic collision terms. Its magnitude can be estimated by equating the right side of (17) (evaluated with f a Maxwellian, $\sigma_{12} = \pi a_o^2$ and $E_{12} = 4\ kT_o(z)$) to $n_o^2\ \phi(T_o)$ and making use of the estimate (McWhirter *et al.*): $\phi(T_o) = 5 \times 10^{-20}\ T_o^{-1/2}$ erg cm^{-1} sec^{-1}, which is claimed to be accurate to within a factor of three for 1.5×10^4 K $\leq T_o \leq 10^7$K. The result is $\eta = 1.9 \times 10^{-6}$.

The electron thermodynamic variables are related to the reference scales T_o, n_o and v_{th} through the following expressions (written for zero average electron velocity):

density:

$$n = n_o \int_{-1}^{1} d\mu \int_0^{\infty} \xi^2\ \phi\ (\mu, \xi, \tau) d\xi \tag{22a}$$

average velocity:

$$\langle v_z \rangle = \frac{n_o v_{th}}{n} \int_{-1}^{1} \mu\ d\mu \int_0^{\infty} \xi^3\ \phi\ (\mu, \xi, \tau)\ d\xi = 0 \tag{22b}$$

internal energy:

$$\frac{1}{2} nm \langle v^2 \rangle \equiv \frac{3}{2} nkT = n_o\ kT_o \int_{-1}^{1} d\mu \int_0^{\infty} \xi^4\ \phi\ (\mu, \xi, \tau)\ d\xi \tag{22c}$$

pressure tensor:

$$\underline{P} = p_{\parallel}\ \hat{e}_z\hat{e}_z + p_{\perp}\ (\hat{e}_x\hat{e}_x + \hat{e}_y\hat{e}_y) \tag{22d}$$

$$p_{\parallel} = mn\ \langle v_z v_z \rangle = 2n_o\ kT_o \int_{-1}^{1} d\mu\ \mu^2 \int_0^{\infty} \xi^4\ \phi\ (\mu, \xi, \tau)\ d\xi \tag{22e}$$

$$p_{\perp} = mn\ \langle v_x v_x \rangle = n_o\ kT_o \int_{-1}^{1} d\mu\ (1 - \mu^2) \int_0^{\infty} \xi^4\ \phi\ (\mu, \xi, \tau)\ d\xi \tag{22f}$$

heat flux:

$$q_z = \frac{1}{2}\ mn\ \langle v^2 v_z \rangle = v_{th}(n_o\ kT_o) \int_{-1}^{1} d\mu\ \mu \int_0^{\infty} \xi^5\ \phi\ (\mu, \xi, \tau)\ d\xi \tag{22g}$$

Finally, I note that if the distribution function is locally Maxwellian with density $n_o(z)$ and temperature $T_o(z)$, its dimensionless form is

$$\phi^*(\mu, \xi, \tau) = \frac{2}{\sqrt{\pi}}\ e^{-\xi^2}\ . \tag{23a}$$

ϕ^* satisfies the normalization

$$\int_{-1}^{1} d\mu \int_0^{\infty} \xi^2\ \phi^*\ (\mu, \xi, \tau)\ d\xi = 1. \tag{23b}$$

When written in terms of the above dimensionless variables the Fokker-Planck equation becomes

$$\mu\xi\left\{\frac{\partial\phi}{\partial\tau} - \frac{\alpha}{2}\left(\xi\frac{\partial\phi}{\partial\xi} + 5\phi\right)\right\} - \beta\left\{\mu\frac{\partial\phi}{\partial\xi} + \frac{1-\mu^2}{\xi}\frac{\partial\phi}{\partial\mu}\right\} = \left.\frac{\delta\phi}{\delta t}\right|_{ee} + \left.\frac{\delta\phi}{\delta t}\right|_{ep} + \left.\frac{\delta\phi}{\delta t}\right|_{inel.} \tag{24a}$$

with

$$\left.\frac{\delta\phi}{\delta t}\right|_{ee} = a\frac{\partial^2\phi}{\partial\xi^2} + b\frac{\partial^2\phi}{\partial\mu\partial\xi} + c\frac{\partial^2\phi}{\partial\mu^2} + d\frac{\partial\phi}{\partial\xi} + e\frac{\partial\phi}{\partial\mu} + p\phi \tag{24b}$$

$$\left.\frac{\delta\phi}{\delta t}\right|_{ep} = \frac{1}{2\xi^3}\frac{n}{n_o}\frac{\partial}{\partial\mu}\left\{(1-\mu^2)\frac{\partial\phi}{\partial\mu}\right\} \tag{24c}$$

$$\left.\frac{\delta\phi}{\delta t}\right|_{inel} = \eta\left\{\frac{(\xi+2)^2}{2\xi}\int_{-1}^{I} d\mu'\ \phi(\mu', \xi+2, \tau) - \xi H(\xi-2)\,\phi(\mu, \xi, \tau)\right\} \tag{24d}$$

The coefficients in (24b) are given in (15a - e) provided $\underline{v}$ and g in latter formulas are replaced by their dimensionless counterparts $\underline{\xi}$ and ℓ, respectively; e.g., $a = \frac{1}{2}\frac{\partial^2\ell}{\partial\xi^2}$. In obtaining (24d) from (16) I have used (18a, b) and have introduced the notation H(x) for the unit step function.

A formula for convenient numerical evaluation of the potential ℓ can be obtained by manipulating the generating function of the Legendre polynomials (Morse & Feshbach 1953, p. 597) to find that

$$|\underline{\xi} - \underline{\xi}'| = \sum_{n=0}^{\infty} A_n(\xi, \xi')\, P_n(\cos\gamma)\ , \tag{25}$$

where γ is the angle between $\underline{\xi}$ and $\underline{\xi}'$ and

$$A_n(\xi, \xi') = -\frac{\xi_>}{2n-1}\left(\frac{\xi_<}{\xi_>}\right)^n\left[1 - \frac{2n-1}{2n+3}\left(\frac{\xi_<}{\xi_>}\right)^2\right]. \tag{26}$$

Here $\xi_>$ is the larger and $\xi_<$ the smaller of ξ and ξ'.

On substituting (25) into (21d) and using the spherical harmonic addition theorem to express $P_n(\cos\gamma)$ in terms of $P_n(\mu)$ and $P_n(\mu')$ I obtain

$$\ell(\mu, \xi, \tau) = \sum_{n=0}^{\infty} \ell^n(\xi, \tau)\, P_n(\mu) \tag{27a}$$

where

$$\ell^n(\xi, \tau) = \frac{2}{2n+1}\int_0^{\infty} \xi'^2\, A_n(\xi, \xi')\, \phi^n(\xi', \tau)\, d\xi' \tag{27b}$$

and

$$\phi^n(\xi, \tau) = \frac{2n+1}{2}\int_{-1}^{1} d\mu'\, P_n(\mu')\, \phi(\mu', \xi, \tau) \tag{27c}$$

In practice, series (27a) converges rapidly because ℓ is determined mainly by the behavior of ϕ at thermal velocities (see 21d), where ϕ remains nearly isotropic. An added virtue of this formulation is that various μ and ξ-derivatives of ℓ, needed for evaluating the coefficients (15a - f), can be obtained analytically from the foregoing formulas, thereby avoiding errors inherent to numerical differentiation.

Auxiliary Conditions

At the boundaries I choose

$$\phi(\mu, \xi, \tau = 0) \equiv \phi_b^+ (\mu, \xi) = \phi^*(\xi) \quad , \quad 0<\mu\leq 1$$

$$\phi(\mu, \xi, \tau = \tau_{max}) \equiv \phi_b^- (\mu, \xi) = \phi^*(\xi) \quad , \quad -1\leq\mu<0 \tag{28}$$

where ϕ^* is a local Maxwellian defined in (23a). This choice can be defended on two grounds beyond simplicity. First, due to the boundaries being located in regions of weak gradients (top) and high density (bottom), I expect the actual incoming distributions to be close to local Maxwellians. Second, I find that a few mean free paths away from the boundaries the computed solution is relatively insensitive choice of $\phi_b^{\pm}$ provided they do not differ significantly from ϕ^*. For example, replacing ϕ^* in (28) by the appropriate Spitzer-Härm distributions has little effect on the computed result in the slab interior. The role of boundary conditions is elucidated in paper II.

Consider now the task of prescribing constraints on the solution in velocity space. To begin, observe that since an electron at rest has no associated direction of flight, ϕ must be single valued at $\xi = 0$, and hence

$$\left.\frac{\partial\phi}{\partial\mu}\right|_{\xi=0} = 0 \text{ for all } \mu, \tau. \tag{29}$$

Two additional constraints one wishes to impose on the solution are that it remain nonsingular (particularly at $\xi = 0$; see Eq. 43) and that it decay at large ξ. Unfortunately, there appears to be no unique way to implement these constraints mathematically. Although the forms chosen below are physically motivated, they are not unique; others could probably serve equally well. Fortunately, numerical experiments show that the solutions are insensitive to the particular forms chosen provided they are sensible expressions of the above physical ideas.

Proceeding, I note that (24a) can be recast as

$$\mu\xi \left\{ \frac{\partial\phi}{\partial\tau} - \frac{\alpha}{2} \left(5\phi + \xi \frac{\partial\phi}{\partial\xi} \right) \right\} = -\frac{\partial}{\partial \underline{\xi}} \cdot \underline{J} \tag{30a}$$

where $\underline{J}$ is the total velocity-space flux density:

$$\underline{J} = \underline{J}_{ce} + \underline{J}_{ep} + \underline{J}_{inel.} - \beta \hat{e}_z \phi \tag{30b}$$

It can be verified that

$$\underline{J}_{es} = \frac{m}{2m_s} \phi \frac{\partial}{\partial \underline{\xi}} \left(\nabla^2_{\underline{\xi}} \ell_s \right) - \frac{1}{2} \frac{\partial^2 \ell_s}{\partial \underline{\xi} \partial \underline{\xi}} \cdot \frac{\partial\phi}{\partial \underline{\xi}} \; ; \; s = e,p \tag{30c}$$

In the following I neglect the contribution of $\underline{J}_{inel.}$ to $\underline{J}$, because it both encumbers the argument and is physically unimportant. Now let V denote a sphere in velocity space centered at the origin with radius ξ_{max}. Integrate (30a) over V, use the divergence theorem, neglect $\underline{J}_{ep} \cdot \hat{e}_\xi = 0\left(\frac{m}{m_p}\right)$, and note that $\beta(\tau)$ has presumably been chosen so that $\int_V d^3\,\underline{\xi}\,\underline{\xi}\,\phi(\underline{\xi}, \tau) = 0$ (zero current condition) to obtain

$$\int_{-1}^{1} d\mu \left[\underline{J}_{ee}(\mu, \xi_{max}) - \left(\beta + \frac{\alpha\,\xi_{max}^2}{2}\right) \phi(\mu, \xi_{max})\, \hat{e}_z \right] \cdot \hat{e}_\xi = 0 , \qquad (31)$$

where τ-dependencies have been suppressed. In order to obtain a constraint on the solution at ξ_{max} I assume that at each τ there are no electrons incident on the spherical surface $\xi = \xi_{max}$ from its exterior; i.e., I assume $\underline{J}_{TOT}(\mu, \xi_{max}) \cdot \hat{e}_\xi \geq 0$ for all μ, where $\underline{J}_{TOT}$ is the bracketed quantity in (31). It then follows that (31) can be satisfied only if the integrand vanishes[1]:

$$\left\{ \underline{J}_{ee} - \left(\beta + \alpha\,\frac{\xi^2}{2}\right) \hat{e}_z\, \phi \right\}_{\xi=\xi_{max}} \cdot \hat{e}_\xi = 0 \ , \text{ all } \mu,\tau. \qquad (32)$$

The stipulation that no electrons be incident on the surface $\xi = \xi_{max}$ from remote regions of velocity space is meaningful provided the actual number of electrons arriving at location τ with energy exceeding $\frac{1}{2}\,m\,v_{max}^2(\tau) = kT_o(\tau)\,\xi_{max}^2$ is negligibly small. A sufficient condition for

1 The term proportional to α in Eq. (32) was inadvertently omitted in calculating the results reported here. I do not believe that this is a serious error.

this to hold is $\xi_{max}^2 \geq 3(T_h/T_c)^{\frac{1}{2}}$ (say), for then there are essentially no electrons anywhere in the atmosphere with energy exceeding $\frac{1}{2} m v_{max}^2$ ($\tau = 0$). For $T_h = 2 \times 10^6$K and $T_c = (8.1 \times 10^3$K) this requires $\xi_{max} \geq 47$. For the present purpose of determining whether significant departures from LTE occur, this estimat proves unnecessarily large, for I find that the computed solution for $\xi < \xi_{max} - 1$ (say) is largely independent of ξ_{max} provided $\xi_{max} \geq 5$. However, the value of ξ_{max} finally adopted, namely $\xi_{max} = 6$, turns out to be too small to accurately determine the electron heat flux in the lower TR.

Again let V denote a spherical volume in velocity space centered at the origin, but now with radius $\xi = \varepsilon << 1$. By integrating (30a) over V, taking the limit $\varepsilon \to 0$, and demanding that ϕ and its derivatives remain bounded as $\xi \to 0$, I deduce that

$$\lim_{\varepsilon \to 0} \int_{-1}^{1} d\mu \left\{ \hat{e}_\xi \cdot \left[\underline{J}_{ee}(\mu, \varepsilon) - \beta \phi(\mu, \varepsilon) \hat{e}_z \right] \right\} = 0 , \tag{33}$$

which states that the <u>net</u> efflux of electrons from the origin is zero. To obtain a constraint on the solution I replace (33) by the stronger requirement that electrons neither enter nor leave velocity space through the origin; i.e.,

$$\lim_{\varepsilon \to 0} \hat{e}_\xi \cdot \left\{ \underline{J}_{ee}(\mu, \varepsilon) - \beta \phi(\mu, \varepsilon) \hat{e}_z \right\} = 0 , \text{ all } \mu, \tau. \tag{34}$$

By expanding expression (30c) for $\underline{J}_{ee}$, Eq. (32) can be brought into the form

$$\left[A_b \frac{\partial \phi}{\partial \xi} + B_b \frac{\partial \phi}{\partial \mu} + C_b \phi \right]_{\xi=\xi_{max}} = 0 \qquad \text{all } \mu, \tau, \tag{35a}$$

where

$$A_b = \frac{\partial^2 \ell}{\partial \xi^2} \quad , \quad B_b = \frac{1 - \mu^2}{\xi^2} \frac{\partial}{\partial \mu} \left[\frac{\partial \ell}{\partial \xi} - \frac{\ell}{\xi} \right] \tag{35b,c}$$

$$C_b = 2\mu \left(\beta + \frac{\alpha \xi^2}{2} \right) - \frac{\partial}{\partial \xi} \left[\frac{1}{\xi^2} \frac{\partial}{\partial \xi} \left(\xi^2 \frac{\partial \ell}{\partial \xi} \right) + \frac{1}{\xi^2} \frac{\partial}{\partial \mu} \left[(1 - \mu^2) \frac{\partial \ell}{\partial \mu} \right] \right] \tag{35d}$$

Equation (34) can be simplified by using (27a) to evaluate $\ell(\mu, v)$ and its derivatives as $\xi \to 0$. The result is

$$\left[D_b \frac{\partial \phi}{\partial \xi} + E_b \phi \right]_{\xi=0} = 0 \ , \qquad \text{all } \mu, \tau \tag{36a}$$

where

$$D_b = \frac{4}{3} I_0^1 - \frac{4}{15} I_2^1 P_2(\mu) \tag{36b}$$

$$E_b = 2\mu \left\{ \beta - \frac{2}{3} I_1^0 \right\} \tag{36c}$$

Here I have used the notation

$$I_m^n = \int_0^\infty \xi^n \, \phi^m(\xi) \, d\xi, \tag{36d}$$

where the ϕ^m are defined in (27c).

Equations (28), (29), (35a-d)[1] and (36a-d) are the auxiliary conditions used in this study. Note that (35a) and (36a) are satisfied identically by $\phi = \phi^*$ if $\alpha = \beta = 0$ and if the coefficients $A_b, \ldots, E_b$ are evaluated for Maxwellian field particles.

As a final remark on auxiliary conditions, I note that Kileen and Mark (1970) have shown that the conditions ($\theta = \cos^{-1} \mu$)

$$\frac{\partial \phi}{\partial \xi} \left(\theta = \frac{\pi}{2}, \; \xi = 0\right) = 0 \tag{37}$$

$$\frac{\partial \phi}{\partial \theta} \left(\theta = 0, \; \xi\right) = \frac{\partial \phi}{\partial \theta} \left(\theta = \pi, \; \xi\right) = 0 \tag{37}$$

are necessary for ϕ to be azimuthally symmetric about $\hat{e}_z$. They also argue that because $\frac{\partial \phi}{\partial \theta} = - \sin \theta \, \frac{\partial \phi}{\partial \mu}$, (37b) does not constraint $\frac{\partial \phi}{\partial \mu}$ at $\mu = \pm 1$, and consequently it is preferable to use θ rather than μ as the independent angular variable. I note, however, that (37b) will be satisfied provided $\frac{\partial \phi}{\partial \mu}$ remains bounded at $\mu = \pm 1$; this latter condition is therefore the appropriate one when using μ as independent variable. I also observe that (36a) reduces to (37a) at $\mu = 0$.

---

[1] See footnote p. 26.

Maxwellian Field Particle Approximation

It will be useful later on to have explicit expressions for the coefficients in (24b) when the potential ℓ is evaluated using $\phi = \phi^*$. This has been referred to earlier as the Maxwellian field particle approximation (MFPA). From (21d) and (23a) I find by straightforward integration that

$$\ell^*(\xi) = \frac{1}{2\pi} \int d^3\underline{\xi}' \, |\underline{\xi} - \underline{\xi}'| \, \phi^*(\xi') \tag{38}$$

$$= \left(\xi + \frac{1}{2\xi}\right) \mathrm{erf}\,(\xi) + \frac{\phi^*}{2}$$

Using this result and equations (15a-e) the coefficients are readily evaluated. I obtain

$$a^* = \frac{\mathrm{erf}(\xi)}{2\xi^3} - \frac{\phi^*}{\xi^2} \tag{39a}$$

$$b^* = 0 \tag{39b}$$

$$c^* = \frac{1 - \mu^2}{2\xi^3} q(\xi) \; ; \; q(\xi) = \left(1 - \frac{1}{2\xi^2}\right) \mathrm{erf}(\xi) + \frac{\phi^*}{\xi} \tag{39c}$$

$$d^* = \frac{q}{\xi^2} \tag{39d}$$

$$e^* = \frac{-\mu q(\xi)}{\xi^3} \tag{39e}$$

$$p^* = 2\psi^* \tag{39f}$$

Neglecting terms of order $e^{-\xi^2}$ in the above coefficients and equating the proton and reference densities leads to the following large-velocity form of the Fokker-Planck equation in the MFPA:

$$\mu\xi\left\{\frac{\partial\phi}{\partial\tau}-\frac{\alpha}{2}\left(5\phi+\xi\frac{\partial\phi}{\partial\xi}\right)\right\}-\beta\left\{\mu\frac{\partial\phi}{\partial\xi}+\frac{1-\mu^2}{\xi}\frac{\partial\phi}{\partial\mu}\right\}=\frac{1}{2\xi^3}\frac{\partial^2\phi}{\partial\xi^2}+\left(\frac{1}{\xi^2}-\frac{1}{2\xi^4}\right)\frac{\partial\phi}{\partial\xi}$$

$$+\frac{1}{\xi^3}\left(1-\frac{1}{4\xi^2}\right)\frac{\partial}{\partial\mu}\left\{(1-\mu^2)\frac{\partial\phi}{\partial\mu}\right\}+\left.\frac{\delta\phi}{\delta t}\right|_{\text{inel.}} \tag{41}$$

To the same approximation the auxiliary condition (35a) is

$$\left\{\frac{1}{\xi}\frac{\partial\phi}{\partial\xi}+\left[2+\mu\xi^2\left(2\beta+\alpha\xi^2\right)\right]\phi\right\}_{\xi=\xi_{max}}=0 \tag{42}$$

For $\xi \ll 1$, the MFPA form of the Fokker-Planck equation is

$$\mu\xi\left\{\frac{\partial\phi}{\partial\tau}-\frac{\alpha}{2}\left(5\phi+\xi\frac{\partial\phi}{\partial\xi}\right)\right\}-\beta\left\{\mu\frac{\partial\phi}{\partial\xi}+\frac{1-\mu^2}{\xi}\frac{\partial\phi}{\partial\mu}\right\}=\frac{2}{\sqrt{\pi}}\left[\frac{1}{3}\frac{\partial^2\phi}{\partial\xi^2}+\frac{2}{3\xi}\frac{\partial\phi}{\partial\xi}+2\phi\right]$$

$$+\frac{2}{\sqrt{\pi}}\left(\frac{1}{3\xi^2}+\frac{\sqrt{\pi}}{2}\frac{1}{\xi^3}\right)\frac{\partial}{\partial\mu}\left[(1-\mu^2)\frac{\partial\phi}{\partial\mu}\right]+\left.\frac{\delta\phi}{\delta t}\right|_{\text{inel.}} \tag{43}$$

Lastly, the MFPA form of the auxiliary condition (36a) is

$$\left[\frac{4}{3\sqrt{\pi}}\frac{\partial\phi}{\partial\xi}+2\mu\beta\phi\right]_{\xi=0}=0 \tag{44}$$

Note that if $\alpha=\beta=\left.\frac{\delta\phi}{\delta t}\right|_{\text{inel.}}=0$, all of the above equations are satisfied by $\phi=\phi^*$.

III. Numerical Method

By now it is perhaps apparent that the central difficulty in this problem lies in devising a means of extracting reliable information from Eq. (24a). The approach outlined here, a doubly iterative, fully implicit, fourth-order finite difference scheme, evolved out of my experience with several simpler but ultimately unsuccessful approaches.

As mentioned earlier, I treat the functional dependence of the coefficients in the differential equation and auxiliary conditions on the distribution function by iteration, starting from the approximation $\phi = \phi^*$ everywhere (MFPA). This is the first of the two levels of iteration referred to above. Its effectiveness is discussed at the end of this section.

My approach to the linear problem has been motivated by the following analogy. Consider (24a) with the inelastic terms omitted for the moment. This equation is of the general form

$$\mu\xi \frac{\partial\phi}{\partial\tau} = (A\,\partial_{\xi\xi} + B\,\partial_{\mu\xi} + C\,\partial_{\mu\mu} + D\,\partial_{\xi} + E\,\partial_{\mu} + G)\,\phi \equiv L\phi \tag{45}$$

where the coefficients depend on μ, ξ, and τ. I find empirically that $A > 0$, $C > 0$, and $4AC - B^2 > 0$ for all μ, ξ, τ, except at $\mu = \pm 1$ where $C = B = 0$. These inequalities can be verified explicitly in the MFPA; their relevance is made clear below. Let $\phi = \phi^+$, $L = L^+$ for $\mu > 0$ and $\phi = \phi^-$, $L = L^-$ for $\mu < 0$ and rewrite (45) as the pair of equations

$$\mu\xi \frac{\partial\phi^+}{\partial\tau} = L^+\,\phi^+ \tag{46a}$$

$$\phi^+(\mu,\xi,\tau = 0) = \phi_b^+(\mu,\xi) \quad , \qquad 0 \le \mu \le 1$$

and

$$\mu\xi \frac{\partial \phi^-}{\partial \tau} = L^- \phi^- \tag{46b}$$

$$\phi^-(\mu,\xi,\tau_{max}) = \phi_b^-(\mu,\varepsilon) \quad , \qquad -1<\mu<0$$

Here I have appended boundary conditions (28) in order to bring out the similarity of these equations to the generalized two-dimensional diffusion equation

$$\frac{\partial \Psi}{\partial t} = (A' \partial_{xx} + B' \partial_{xy} + C' \partial_{yy} + D' \partial_x + E' \partial_y + G')\Psi \; ; \; (x,y) \in R, \; t>0$$

$$A'>0 \; , \; C'>0 \; , \; 4A'C' - B'^2>0 \; , \text{ all } (x,y) \in R \tag{47}$$

$$\Psi(x,y,t=0) = \Psi_o(x,y) \quad ,$$

where t is time, R is a region of the x-y plane, and where now the inequalities assure that the equation is parabolic (see, e.g. Carrier and Pearson 1976, p. 266). This latter statement implies that Eq. (47) can be stably integrated forward, but not backward in time. Intuitively speaking, this is because the differential operator on the right in (47) is a smoothing operator; its action on a spatially localized function produces a less localized one. Hence distinct initial configurations, $\Psi_0(x,y)$, evolve into a similar ones as time progresses. Any attempt to reverse this evolution is therefore unstable.

In our case the spatial variable $ds = \frac{d\tau}{\mu}$ plays a role analogous to time in (47), while the velocity variables μ and ξ are analogous to x and y. Equation (46a) is integrated forward in τ, starting from the boundary condition at $\tau = 0$; Eq. (46b), on the other hand, is integrated backwards in τ, starting from the boundary condition at τ_{max}. An essential complication exists, however, in that the two equations are coupled through continuity requirements on ϕ and its μ-derivatives at $\mu = 0$. Fortunately, this complication is readily handled at the difference-equation level.

Consider a centered, three-point difference approximation to $\frac{\partial^2 \phi^-}{\partial \mu^2}$ near $\mu = 0$. Choose an equally spaced mesh on [-1,1] with mesh width $\Delta\mu = 2.0/(NA-1)$, where NA is an even integer. Let $k_o = NA/2$ and label points so that $-1 \leq \mu_1, \ldots, < \mu_{k_o} < 0 < \mu_{k_o+1}, \ldots, < \mu_{NA} \leq 1$. (Note that $\mu = 0$ is not a mesh point.) Then

$$\left.\frac{\partial^2 \phi^-}{\partial \mu^2}\right|_{\mu=\mu_{k_o}} = \frac{\phi^-_{k_o-1} - 2\phi^-_{k_o} + \phi^+_{k_o+1}}{(\Delta\mu)^2},$$

where ϕ_k means $\phi(\mu_k)$. Other μ-derivatives at mesh points adjacent to $\mu = 0$ are handled in a similar way.

It is now not difficult to see that if the μ and ξ-derivatives in Eqs. (46a, b) and side conditions (38c, d) are replaced by difference quotients, with μ-derivatives at mesh points near $\mu = 0$ treated as shown above and those near

$\mu = \pm 1$ approximated by one-sided differences, the resulting difference equations can be cast in the matrix form

$$\frac{\partial \underline{\phi}^-}{\partial \tau} = \underline{\underline{M}}^- \underline{\phi}^- + \underline{\underline{N}}^- \underline{\phi}^+ \quad , \qquad -1 \leq \mu < 0 \tag{48a}$$

$$\frac{\partial \underline{\phi}^+}{\partial \tau} = \underline{\underline{M}}^+ \underline{\phi}^+ + \underline{\underline{N}}^+ \underline{\phi}^- \quad , \qquad 0 < \mu \leq 1 \tag{48b}$$

where I have divided (46a,b) by the product $\mu\xi \neq 0$. Here $\underline{\phi}^{\pm}(\tau)$ are vectors of length k_o x NV, where NV is the number of uniformly spaced velocity points. Elements of $\underline{\phi}^{\pm}$ are ordered so that all angle points at a given velocity are adjacent; i.e., for $1 \leq k \leq k_o$, the $(k + (j - 1)\, k_o)^{th}$ element of $\underline{\phi}^-$ is $\phi(\mu_k, v_j, \tau)$, and for $k_o + 1 \leq k \leq NA$, the $(k - k_o + (j - 1)\, k_o)^{th}$ element of $\underline{\phi}^+(\tau)$ is $\phi(\mu_k, v_j, \tau)$. $\underline{\underline{M}}^{\pm}$ and $\underline{\underline{N}}^{\pm}$ are square matrices of order k_o x NV, and, for three-point velocity differences, are block-tridiagonal in form.

Equations (48a) and (48b) are now solved by iteration. One starts with an initial estimate of $\underline{\phi}^-$, say $\underline{\phi}^- = \underline{\phi}^*$, uses this estimate to evaluate the term $\underline{\underline{N}}^+ \underline{\phi}^-$ appearing on the right in (48b) for all τ, and then integrates the resulting inhomogeneous equation forward in τ, starting from $\tau = 0$, where $\underline{\phi}^+ = \underline{\phi}_b^+$, and ending at $\tau = \tau_{max}$. The $\underline{\phi}^+$ so obtained is then used to evaluate the term $\underline{\underline{N}}^- \underline{\phi}^+$ appearing on the right in (48a), and the resulting inhomogeneous equation is integrated backward from τ_{max} to $\tau = 0$. The process is then iterated to convergence.

Figure 1 illustrates how this scheme works in practice. There I plot successive approximations to $\phi(\mu)$ at fixed $\xi(= 5.48)$ and $\tau(= 147; T_o(\tau) = 5.28 \times 10^5 K)$ for a TR model with $P = P_o/2$. The numbers labeling curves denote iteration number. Thus, "0" is the initial estimate $\phi^*(\xi = 5.48)$, "1" is the result of the first forward pass, "2" is the result of the first backward pass,

and so on. The curve labeled "15" is the result of seven-and-a-half full iterations; as seen, it is remarkably smooth. Behavior at other depths and other velocities is similar. A summary of my experience with this iterative process is the following. The first few passes produce large relative changes in the solution. After ten or so iterations the largest relative change between iterates is generally a few percent; after twenty it is a few tenths of a percent. Thereafter the rate of convergence is slower.

In practice the iteration is stopped when the largest relative correction to the previous iterate is a few tenths of a percent, as this is estimated to be the level of the overall truncation error.

Consider now what turns out to be the crux of the numerical problem, namely choice of a spatial-differencing scheme. By analogy with the situation for time-differencing Eq. (47), there are three classes of method available (see e.g., Richtmyer and Morton, 1967): explicit, alternating direction implicit (hereafter ADI), and fully implicit differencing. Note that the computational cost per step of these methods increases sharply in order listed. Pertinent aspects of the problem to be considered in choosing among these are: a) our interest in long "integration times" - τ_{max} can be as large as 10^3; b) the necessity of storing the solution, typically 1.5×10^4 numbers per depth; and c) the strong velocity dependence of the coefficients in the differential equation; in particular, their singular behavior as $\xi \to 0$. Factors (a) and (b) imply that methods requiring a small step size, although perhaps competitive from the standpoint of computation time, may be unsuitable due to storage limitations. Indeed, due to (c), this situation actually arises for both explicit and ADI difference schemes (see below).

In practice, then, only fully implicit schemes have proven effective, essentially because only these permit use of step sizes large enough for the calculation to be feasible. The situation is summarized by the following estimates of the maximum local step size $\Delta\tau$ allowed by the different methods:

$$\Delta\tau < 0\left[(\Delta\mu)\quad(\Delta\xi)^2\right] \quad , \quad \text{explicit} \tag{49a}$$

$$\alpha(\tau)\Delta\tau < 0\left[\Delta\mu\ (\Delta\xi)^3\right]^{1/2} \quad , \quad \text{ADI} \tag{49b}$$

$$\alpha(\tau)\Delta\tau < 1 \quad , \quad \text{fully implicit.} \tag{49c}$$

Arguments supporting (49a,b) are given in the Appendix. Suffice it here to say that (49a) arises from stability considerations, while (49b) is a necessary condition for the difference between ADI and fully implicit approximations to the spatial derivative term be uniformly small. Since $\Delta\mu \approx \Delta\xi \approx 0.025$, and in light of (a) and (b) above, it is clear that neither explicit nor ADI schemes are suited for this problem. Condition (49c), on the other hand, derives from the underlying physics as can be seen from the following argument.

As discussed in the introduction, electrons at location τ are collision-dominated for velocities such that $\alpha(\tau)\xi^4 < 1$. In this regime the distorting effect of gradients and electric field on the distribution function is mediated by velocity-space derivative terms proportional to α and β on the left in (24a); the $\frac{\partial\phi}{\partial\tau}$ term is unimportant. Thus, at low velocities the equation is local in τ, but is non-local in velocity space. On the other hand, for large velocities ($\alpha\xi^4 >> 1$) electrons traverse many temperature scale lengths before thermalizing and the equation becomes spatially non-local. Since the $\frac{\partial\phi}{\partial\tau}$ term first becomes important at $\xi_c = \alpha^{-1/4}$, one expects the largest allowable step size to be comparable to the mean free path evaluated at ξ_c; i.e.,

$\Delta z \lesssim \lambda(\xi_c) = \left(\frac{d \ln T}{dz}\right)^{-1}$, or equivalently, $\alpha\Delta\tau \leq 1$. Since α is quite small for conditions of interest (Table 1), it should be possible to construct models using a modest number of depth points. As mentioned, only fully implicit differencing allows one to realize this possibility.

Unfortunately, the computational cost per step of fully implicit differencing is substantial, for at each depth one must solve a large system of linear equations. For three-point difference approximations to ξ-derivatives these equations are block-tridiagonal in form. Attempts to solve these equations using iterative techniques (successive block over-relaxation and ADI iteration) proved unsuccessful, due partly, no doubt, to my inability to find good acceleration parameters for either method, but due also, in part, to a more fundamental reason. Inspection of (41) reveals that the first μ and v-derivative terms become dominant at large velocities. If these are approximated using centered differences, as is desirable from the standpoint of accuracy, the associated difference matrix becomes off-diagonally dominant, and hence ill-suited for treatment by iterative methods.

I was thus led to adopt the direct method of block-triangular-factorization (block LU-decomposition). In addition to allowing one to obtain accurate solutions to the difference equations in routine fashion, this approach has the virtue of permitting many (up to 30, say) forward-backward iterations to be performed at a cost not substantially greater than that of a single pass. This is because the amount of computation required to factor the original matrix at a given depth is far greater than needed to solve the two resulting block-triangular systems. Disadvantages of the direct approach, however, are that it requires extensive disk storage space and that, unless carefully coded, the calculation can become I/O bound during the solution phase of execution.

Unfortunately, when the above scheme was implemented using second-order, centered difference approximations for all derivatives, and run on the finest mesh storage capabilities would permit, it gave inaccurate results. Subsequent investigation showed, however, that accuracy could be improved substantially by going to higher-order differences. I was thus led to the following difference approximation to (45) at interior mesh points:

$$\mu_k \xi_j \, \delta^4_{\tau+} \left\{\phi^i_{jk}\right\} = \left(A\, \delta^4_{\xi\xi} + B\, \delta^4_{\xi} \delta^4_{\mu} + C\, \delta^6_{\mu\mu} + D\, \delta^4_{\xi} + E\, \delta^6_{\mu} + G\right) \left\{\phi^i_{jk}\right\} \tag{50}$$

$$\mu_k > 0, \quad i \geq 5, \quad k_o \leq k < NA-3, \quad 3 < j < NV-2$$

Here ϕ^i_{jk} means $\phi(\mu_k, \xi_j, \tau_i)$, all coefficients are evaluated at the point (μ_k, ξ_j, τ_i), and the difference operators are defined as follows:

$$\delta^4_{\tau+} \left\{\phi^i_{jk}\right\} = (24\, \Delta\tau)^{-1} \left[50\, \phi^i - 96\, \phi^{i-1} + 72\, \phi^{i-2} - 32\, \phi^{i-3} + 6\, \phi^{i-4}\right] \tag{51a}$$

$$\delta^4_{\xi} \left\{\phi^i_{jk}\right\} = (12\, \Delta\xi)^{-1} \left[\phi_{j-2} - 8\, \phi_{j-1} + 8\, \phi_{j+1} - \phi_{j-2}\right] \tag{51b}$$

$$\delta^4_{\xi\xi} \left\{\phi^i_{jk}\right\} = \left(12(\Delta\xi)^2\right)^{-1} \left[-\phi_{j-2} + 16\, \phi_{j-1} - 30\, \phi_j + 16\, \phi_{j+1} - \phi_{j+2}\right] \tag{51c}$$

$$\delta^6_{\mu} \left\{\phi^i_{jk}\right\} = (60\, \Delta\mu)^{-1} \left[-\phi_{k-3} + 9\, \phi_{k-2} - 45\, \phi_{k-1} + 45\, \phi_{k+1} - 90\, \phi_{k+2} + \phi_{k+3}\right] \tag{51d}$$

$$\delta^6_{\mu\mu} \left\{\phi^i_{jk}\right\} = \left[180(\Delta\mu)^2\right]^{-1} \left[2\phi_{k-3} - 27\, \phi_{k-2} + 270\, \phi_{k-1} - 490\, \phi_{k+1}\right. \tag{51e}$$

$$\left. - 27\, \phi_{k+2} + 2\, \phi_{k+3}\right]$$

Here unneeded subscripts and superscripts have been omitted. Superscripts on the δ's denote the order of the associated truncation error.

Calling the right side of (50) ψ^i_{jk}, I write the difference equations for grid points near the lower boundary as:

$i = 2, 3, \mu_k > 0$

$$\mu_k \xi_j \left(\frac{\phi^i - \phi^{i-1}}{\Delta\tau} \right) = \frac{1}{2} \left(\psi^i_{jk} - \psi^{i-1}_{jk} \right) \tag{52a}$$

$i = 4, \mu_k > 0$

$$\frac{\mu_k \xi_j}{6\Delta\tau} (11\ \phi^i - 18\ \phi^{i-1} + 9\ \phi^{i-2} - 2\ \phi^{i-3}) = \psi^i_{jk} \tag{52b}$$

For the μ-derivatives near end points I use centered fourth-order formulas at μ_{NA-2}, and one-sided fourth-order formulas at μ_{NA-1} and μ_{NA}. ξ-derivatives at $\xi = \Delta\xi$ and $\xi_{max} - \Delta\xi$ are approximated by centered second-order formulas, and at $\xi = 0$, ξ_{max} by one-sided second-order formulas. Use of these second-order formulas does not seem to have degraded the overall fourth-order accuracy.

The foregoing difference equations, together with their counterparts for $\mu < 0$ and difference approximations to the subsidiary conditions (42) and (44), can be written in matrix notation as:

$$\underline{\underline{M}}^+_i \underline{\phi}^+_i = \underline{q}^+_i - \underline{\underline{N}}^+_i \underline{\phi}^-_i \ , \qquad \mu>0,\ i=2, \ldots, ND \tag{53a}$$

$$\underline{\underline{M}}^-_i \underline{\phi}^-_i = \underline{q}^-_i - \underline{\underline{N}}^-_i \underline{\phi}^+_i \ , \qquad \mu<0,\ i=ND-1, \ldots, 1 \tag{53b}$$

Here ND is the number of depths and the vectors $\underline{q}_i^{\pm}$ represent that part of the spatial derivative term depending on $\underline{\phi}_\lambda^{\pm}$ for $\lambda < i$ ($\mu > 0$) or $\lambda > i$ ($\mu < 0$); at any stage of the calculation the $\underline{q}^i$ are therefore known vectors. The origin of matrices $\underline{\underline{N}}_i^{\pm}$ and the ordering of elements of $\underline{\phi}_i^{\pm}$ has been discussed in the lines following (48b). Matrices $\underline{\underline{M}}_i^{\pm}$ are of order k_o x NV (recall k_o = NA/2) and are block-pentadiagonal in form;

$$\underline{\underline{M}}_i^{\pm} = \begin{bmatrix} \underline{\underline{C}}_1 & \underline{\underline{D}}_1 & \underline{\underline{E}}_1 & & & & \\ \underline{\underline{B}}_2 & \underline{\underline{C}}_2 & \underline{\underline{D}}_2 & \underline{\underline{E}}_2 & & 0 & \\ \underline{\underline{A}}_3 & \underline{\underline{B}}_3 & \underline{\underline{C}}_3 & \underline{\underline{D}}_3 & \underline{\underline{E}}_3 & & \\ & \ddots & & \ddots & & \ddots & \\ & 0 & & & & \underline{\underline{E}}_{NV-2} & \\ & & & & & \underline{\underline{D}}_{NV-1} & \\ & & & & \underline{\underline{A}}_{NV} & \underline{\underline{B}}_{NV} & \underline{\underline{C}}_{NV} \end{bmatrix}$$

The submatrices $\underline{\underline{A}}_j$, .., $\underline{\underline{E}}_j$ are square and of order k_o; in general, they are all bandmatrices with bandwidth seven. In the MFPA, however, off-diagonal submatrices are diagonal due to the absence of the mixed derivative term from (45).

From the defining relation $\underline{\underline{M}}_i^{\pm} = \underline{\underline{L}}_i^{\pm}\underline{\underline{U}}_i^{\pm}$ it is easily found that

$$\underline{\underline{L}}_i^{\pm} = \begin{bmatrix} \underline{\underline{I}} & & & \\ \hat{\underline{\underline{B}}}_2 & \underline{\underline{I}} & & \\ \hat{\underline{\underline{A}}}_3 & \hat{\underline{\underline{B}}}_3 & \underline{\underline{I}} & 0 \\ & \ddots & \ddots & \ddots \\ & 0 & & \underline{\underline{I}} \\ & & \hat{\underline{\underline{A}}}_{NV} & \hat{\underline{\underline{B}}}_{NV} \end{bmatrix} \quad ; \quad \underline{\underline{U}}_i^{\pm} = \begin{bmatrix} \hat{\underline{\underline{C}}}_1 & \hat{\underline{\underline{D}}}_1 & \underline{\underline{E}}_1 & & 0 \\ & \hat{\underline{\underline{C}}}_2 & \hat{\underline{\underline{D}}}_2 & \underline{\underline{E}}_2 & \\ & & \ddots & \ddots & \ddots \\ & 0 & & & \underline{\underline{E}}_{NV-2} \\ & & & & \hat{\underline{\underline{D}}}_{NV-1} \\ & & & & \hat{\underline{\underline{C}}}_{NV} \end{bmatrix}$$

where the submatrices are again square and of order k_o and $\underline{\underline{I}}$ is the identity matrix. We note that although the original $\underline{\underline{A}}_j$, $\underline{\underline{B}}_j$, ..., are sparse, their counterparts $\hat{\underline{\underline{A}}}_j$, $\hat{\underline{\underline{B}}}_j$ (except $\hat{E}_j = E_j$) are, in general, dense.

Several comments concerning my choice of difference formulas are in order. First, I note that the submatrices in $\underline{\underline{U}}_i$ and $\underline{\underline{L}}_i$ fill regardless of the bandwidth of the submatrices in $\underline{\underline{M}}_i$. Computation and storage requirements are therefore largely independent of the order of μ-difference formulas. In addition to small truncation errors, the chosen seven-point formulas afford enhanced coupling between positive and negative μ-components of the solution. Similarly, the use of five-level spatial differences entails less storage and computation than do centered, second-order formulae, yet offer smaller truncation errors. Unfortunately, going from three to five-point velocity differences costs dearly; for a fixed number of velocity mesh points, disk storage doubles and computation increases by roughly a factor of 2.5. Nevertheless, I find that the increased accuracy of the fourth-order method more than compensate for the added storage requirements per point.

The author has recently learned that it is possible to difference (45) in such a way as to obtain fourth-order accurate approximations to the μ and ξ-derivatives and yet have the associated difference matrices, $\underline{\underline{M}}_i^{\pm}$, be block-tridiagonal. This procedure is being tested and if proven effective will be used in future versions of the present code. Also, newly developed iterative methods for solution of non-symmetric sparse matrices (Manteuffel 1977, Kershaw 1977, Van Der Vorst 1981) appear promising.

An overview of the linear problem can be had by viewing its global matrix structure:

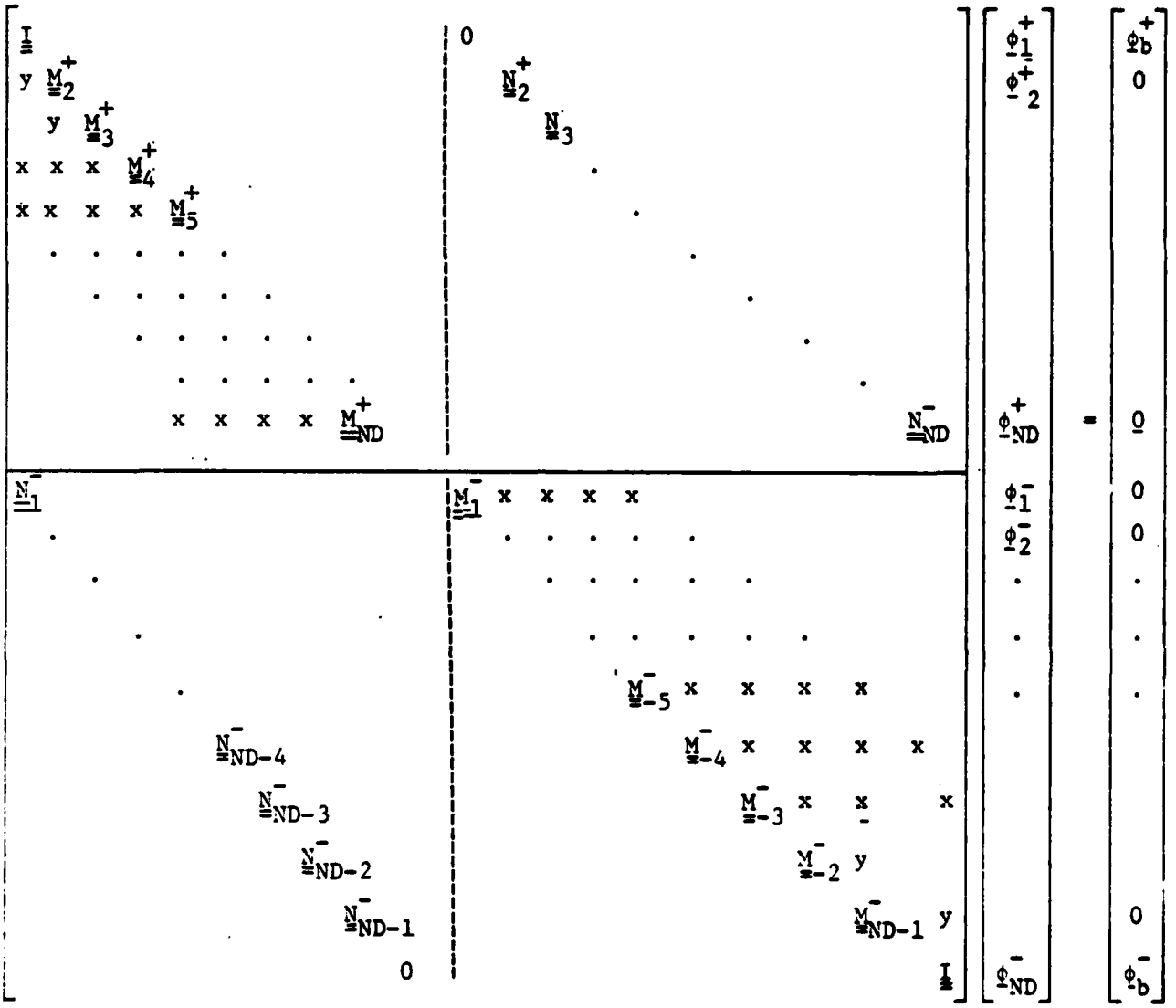

(54)

Here $\underline{\underline{I}}$ is the k_o x NV identity matrix, $\underline{\phi}_b^{\pm}$ are vectors containing grid point values of the boundary conditions, x's denote diagonal matrices originating from one-sided difference approximations to the spatial derivative term, and the y's are band matrices originating from our use of centered space differences at i = 2,3 ($a > 0$) and at i = ND-1, ND-2 ($a < 0$).

The forward-backward iteration described earlier is now seen to be the obvious approach to the iterative solution of the above matrix equation.

The above procedure has been programed and tested on the Cray-1 computer at the National Center for Atmopsheric Research. Due to the predominance of matrix manipulations the algorithm is ideally suited to the vector processing capabilities of the Cray-1. In fact, essentially all of the "hard" computation is performed using assembly-language routines designed to utilize the vector character of the machine to the fullest possible extent. Results presented in the following section were obtained using 71 depths, 60 angles and 256 velocities. For this number of points approximately six minutes of central processor time is required to setup and solve the matrix equation (54), using 30 forward-backward passes. Storing the triangular factors of the $\underline{\underline{M}}_i^{\pm}$ matrices requires $2 \times (ND-1) * NV * 4 * k_o * (k_o + 7) \approx 1.6 \times 10^8$ words of disk space. High disk-to-central memory data transfer rates are obtained by using four independent data channels and a double buffering scheme.

The code was tested in three ways: first, it was verified that starting from a distribution markedly different than Maxwellian, the calculation would converge to an absolute Maxwellian in an isothermal and isobaric atmosphere ($A(\tau) = B(\tau) = 0$) with Maxwellian boundary conditions. Second, it was verified that the Spitzer-Härm solution could be reproduced in a high pressure atmosphere. Four coefficient iterations were required to obtain an accuracy of five percent or better for $\xi \leq 3.2$. Finally, the accuracy of calculation under realistic conditions was checked by observing the effect of judiciously refining the mesh. For this purpose a word-packing routine was used to effectively double the amount of disk storage available. Unfortunately, use of this routine proved far too costly for it to be used for other than testing purposes.

As a result of these tests I judge the results presented below to have a relative accuracy of ten percent or better.

I turn now to the promised discussion of the effectiveness of treating the quasi-linear collision term by iteration under realistic conditions. Table 2a is a tabulation, for three coefficient iterations, of the zeroth and first angular moments of the distribution (cf. 27c), normalized to ϕ^*, at a location near the bottom of our standard model ($\tau \approx 27$, $T_o(\tau) = 19900K$, $\alpha(\tau) = 3.8 \times 10^{-2}$). The calculation was started from LTE so that the first iterate corresponds to the MFPA. The points to note regarding Table 2a are: a) the largest relative change in ϕ^o between the first and third iterates is less than four percent for all $\xi \leq 5.5$. b) the same is true for ϕ^1 for $\xi_c < \xi \leq 5.5$. ($\xi_c = \alpha^{-1/4} \approx 2.3$). and c) ϕ^1 fluxuates widely between iterates at thermal velocities. On the basis of these and more detailed comparisons, I infer that ϕ^o at all ξ, and the entire distribution function at suprathermal velocities, can be obtained with good accuracy in the MFPA. What cannot be obtained correctly in this approximation are quantities which depend sensitively on the pitch angle distribution of thermal electrons; for example, the heat flux. This is illustrated by Table (2b) giving the dimensionless heat flux, $\frac{2}{3}\int_o^\infty \xi^5 \phi^1(\xi, \tau)\, d\xi$, for each iteration together with its Spitzer-Härm value.

I close this section by mentioning two simplifications which have been useful. First, I evaluate the troublesome inelastic term (24d) iterativelv. during the course of the forward-backward iteration. Second, I determine the polarization electric field required for zero current flow using the Spitzer-Härm (1953) result $\beta = 0.35\,\alpha$. This value of β gives zero mean electron velocities to well within the accuracy of the calculation.

IV. Numerical Results

Results are presented for two model transition regions, one with electron pressure $\langle n_o T_o \rangle = 6 \times 10^{14}$ cm^{-3} K $\equiv P_o$ and the second at $P_o/2$. I note that although P_o is the most frequently quoted electron pressure for the spatially averaged quiet sun TR (e.g., Dupree 1972), different EUV observations yield pressures which can differ from P_o by at least a factor of two (Withbroe 1978). Both models span the temperature range 8100 - 2×10^6 K and have a thickness of 5×10^4 km. The distribution function has been calculated in the MFPA for the boundary conditions (28) using $\xi_{max} = 6$ and a grid of 256 velocities, 71 depths and 60 angles.

a) Reference Atmosphere

A portion of the reference atmosphere obtained by solving Eq. (20) with $\langle n_o T_o \rangle = P_o$ is given in Table 3, where λ is the thermal mean free path, q_{sh} the Spitzer-Härm heat flux, and Q_{rad} the radiative losses per unit volume per unit time calculated from McWhirter et. al's (1975) loss function. Two points concerning this table should be noted. First, from the near constancy of q_{sh} above roughly 20,000 K one can infer that radiative losses have a negligible effect on the temperature profile above this level. Consequently $T_o(z)$ for the $P_o/2$ case is very similar to that for P_o and values of the parameter α are roughly double those for the P_o case. Second, relative to empirical models (e.g., Vernazza et al. 1973, Gouttebroze and Leibacher 1980), the calculated temperature gradient is probably too steep below 60,000 K, and is certainly so below 30,000 K. This discrepancy illustrates the known result (Withbroe 1977, Pneuman and Kopp 1978, Athay 1981) that the empirical temperature profile of the low TR in either the quiet sun or in active region loops cannot be understood on the basis of models whose energy budget includes

only (classical) thermal conduction and radiation. However, in the present context this discrepancy is irrelevant because, as mentioned earlier, $T_o(z)$ serves only to define the relationship between dimensional and dimensionless variables; the true temperature profile is determined self-consistently from the Fokker-Planck equation and, in principle, is independent of $T_o(z)$. This is not wholly the case here because radiative losses are (incorrectly) evaluated on the $T_o(z)$ scale and, moreover, are assumed to have the same functional dependence on temperature as in (electron) LTE.

b) Thermodynamic Quantities

Typical values of the reduced density, temperature, mean velocity, and the ratio of parallel to perpendicular pressures are listed in Table 4 (see Eqs. 22 a-f). Points of interest are that: a) the Spitzer-Härm value for the polarization electric field gives adequately small mean electron velocities in the MFPA. b) Below it will be seen that the tail of the distribution is highly anisotropic (Fig. 5). Nevertheless, the ratio $p_{||}/p_{\perp}$ remains within a few percent of unity. Whether this remains true when the calculations are carried to larger velocities remains to be determined. c) The ratio T/T_o is seen to be slightly larger than unity in the lower atmosphere. No quantitative significance should be attached to this temperature rise however, because the heat flux in the present calculation is inaccurate due to my use of the MFPA and to truncation of the calculation at $\xi_{max} = 6$. The latter shortcoming appears especially serious in light of recent calculations using the Bhatnaghar, Gross and Krook equation (Shoub 1982; Paper II), which indicate that a substantial part of the energy flux into the low TR is carried by superthermal electrons with velocities 10-30 times local thermal velocities. Thus, the correct (kinetic-theoretical) temperature profile of the TR remains to be determined.

Finally, I note that although the calculated T(z) is inaccurate low in the atmosphere, this does not imply that the calculated distribution function (see below) is grossly in error in this region. In all likelihood it is not, especially at suprathermal velocities, because the tail of the distribution in the low TR is largely independent of the local temperature structure.

c) Distribution Function

The isotropic part of the dimensionless distribution function, $\phi^{o}(\xi, T_o) \equiv \frac{1}{2}\int_{-1}^{1} d\mu\ \phi(\mu, \xi, T)$, is shown at several heights for the case $P = P_o$ in Fig. 2, and in more detail in Table 5. The effect on ϕ° of reducing the pressure a factor of 2 is also illustrated in Table 5. The dimensional distribution $f^{o}(v, T_o)$ $(n_o/2\pi\ v_{th}^3)\ \phi^{o}(\xi, T_o)$ is shown in Fig. 3 for the case $P = P_{o/2}$. For comparison a local-Maxwellian distribution is shown as a dashed line in Figures 2 and 3.

The essential results here are that, relative to a local-Maxwellian, the tail of the distribution is highly overpopulated and exhibits only a weak spatial (temperature) dependence throughout the lower TR and chromosphere. From Table 5 it can be seen that, with respect to normalization, the enhanced tail is compensated for (approximately) by a suppression of ϕ below ϕ^* for $1.5 < \xi < 2.5$ For temperatures less than approximately 10^5K, ϕ° begins to exceed ϕ^* at about $\xi = 2.5$. Higher in the atmosphere ϕ° remains close to ϕ^* out to progressively larger ξ. An analytical characterization of $\phi^{\circ}(\xi, T_o)$ is obtained in paper II.

Fig. 4 shows the 1-dimensional distribution

$$\phi_z(\xi_z, T_o) \equiv \int_{-1}^{1} d\mu \int_{o}^{\infty} \xi^2\, \delta(\xi_z - \mu\xi)\, \phi(\mu, \xi, T_o)\, d\xi$$

$$= \int_{|\xi_z|}^{\infty} \xi\, \phi(\xi_z/\xi, \xi, T_o)\, d\xi$$

at several heights, including the boundaries. Here $\xi_z = \underline{\xi} \cdot \hat{e}_z$. A Maxwellian is again shown as a dashed line for comparison.

Note the asymmetry between directions parallel ($\xi_z>0$) and anti-parallel to ∇T. Unfortunately, the structure in ϕ_z for $\xi_z>0$, evident in Fig. 4 at T_o = 19,900 K and 1.05 x 10^5 K, is artificial--an artifact of my setting $\phi(\frac{\xi_z}{\xi}, \xi) = 0$ for $\xi > 6$ in the above integral for ϕ_z. This procedure is inaccurate for $\xi_z \geq 3$ because the pitch angle distribution (Fig. 5, $\mu > 0$) is such that for $\xi \geq 3$, $\phi(\frac{\xi_z}{\xi}, \xi)$ decreases slowly with increasing ξ.

Finally, I note that ϕ_z differs from ϕ_z^* at thermal velocities, but the differences are too small to be noticeable in Fig. 4.

Fig. 5 shows the pitch angle dependence of the distribution for a sequence of velocities at a location near the bottom of the TR for the case $\langle n_o T_o \rangle = P_o/2$. The main features of these plots are the following. At low velocities deviations from isotropy are small and, moreover, ϕ varies linearly with μ, as predicted by classical theory. The flux of low velocity electrons is directed upward, toward higher temperatures. This upward drift has two causes; natural (concentration) diffusion due to a negative gradient in the number of low velocity electrons ($\frac{d\ln f}{dz} \simeq \frac{d\ln f^*}{dz} \simeq (\xi^2 \frac{5}{2}) \frac{d\ln T_o}{dz}$), and forced diffusion driven by the polarization electric field. Evidently, for some ξ between 1.75 and 2, $\frac{d\ln f}{dz}$ becomes positive and sufficiently large that, in response, suprathermal electrons diffuse downward against the action of the field. This effect becomes more pronounced with increasing ξ, leading to the strong anisotropy evident in the bottom two panels of Fig. 5. Note that for $\xi \geq 3$, $\phi(\mu, \xi)$ decreases relatively slowly with increasing μ for $-1 \leq \mu_o(\xi)$, where $\mu_o(\xi=3) \simeq .5$ and $\mu_o(\xi = 4) \simeq .4$, and then decreases more rapidly for $\mu_o(\xi) < \mu \leq 1$. That the changeover occurs at $\mu_o(\xi) > 0$, and not at $\mu = 0$, is due to pitch angle (back) scattering.

Fig. 6 is a contour plot of the distribution function at a location near the bottom of the TR for the case $P = P_o$. From this plot it is clear that the propagation of electrons down the gradient is diffusive rather than beam-like in character.

d) Effect on Collision Rates

From the standpoint of spectroscopic diagnostics, the main consequence of having an overpopulated tail on the electron energy spectrum is that it causes an increase in electron-ion collision rates and an attendant alteration of an element's ionization balance and, possibly, its line emission. I illustrate these effects here for magnesium and for helium, but stress that the results are preliminary due to shortcomings in both my calculation of the distribution function and ionization equilibrium (see below).

i) Magnesium

The expression for the collisional ionization rate per ion is

$$C_{1\kappa}(T) = 4\pi \int_{v_{1\kappa}}^{\infty} v^3 \, \sigma_{1\kappa}(v) \, f^{\circ}(v) \, dv$$

$$= 2 \, n_o v_{th} \int_{\xi_{1\kappa}(T)}^{\infty} \xi^3 \, \sigma_{1\kappa}(v_{th}\xi) \, \phi^{\circ}(\xi, T) \, d\xi$$

where $\sigma_{1\kappa}$ is the ionization cross section, $v_{1\kappa}$ is the electron-threshold velocity, and $\xi_{1\kappa} = v_{1\kappa}/v_{th}$. The corresponding rate based on a Maxwellian, denoted $C_{1\kappa}^{*}$, is easily shown to be

$$C_{1\kappa}^{*}(T) = n \, C_o \sqrt{T} \, \exp(-E_{1\kappa}/kT) \, \Gamma(T)$$

where C_o is a constant, $E_{1\kappa} = 1/2\ m\ v_{1\kappa}^2$ and

$$\Gamma(T) = \int_o^\infty (x + \frac{E_{1\kappa}}{kT})\ \sigma_{1\kappa}\ (E_{1\kappa} + xkT)\ e^{-x}\ dx$$

is slowly varying. In Table 6 I list $\xi_{1\kappa}$ and the ratio $C_{1\kappa}/C_{1\kappa}^*$ for the first six ionization stages of magnesium. $C_{1\kappa}$ was calculated numerically using the FP results for ϕ° and the cross section from Allen (1976 p. 41). There are no entries for $\xi_{1\kappa} > 5.4$ because ϕ° was calculated only out to $\xi_{max} = 6$. The salient aspects of these results are: a) $C_{1\kappa}/C_{1\kappa}^* \approx 1$ when $\xi_{1\kappa}$ is below a critical value increasing from roughly 2.0 at $T \simeq 10^4$ K to 2.5 at $T \simeq 10^5$ K. b) Once $\xi_{1\kappa}$ is larger than this critical value $C_{1\kappa}/C_{1\kappa}^*$ increases exponentially with decreasing temperature, and c) once $C_{1\kappa}/C_{1\kappa}^* >> 1$ at a given temperature, the ratio is then strongly density dependent. These results simply reflect the behavior of the calculated distribution function: (a) holds because $\phi^o(\xi,T_o) \approx \phi^*(\xi)$ for $\xi < \xi_c$ and ξ_c increases with T_o; (b) holds because at low temperatures the tail of the dimensional, angle-averaged distribution, and hence $C_{1\kappa}^*$, has only a weak spatial dependence (Fig. 3) whereas $C_{1\kappa}$ decreases exponentially with decreasing temperature; (c) simply reflects the density (or pressure) dependence of the tail, as shown in Table 5.

Figure 7 shows how the enhanced ionization rates affect the ionization balance of Mg. Processes included in the ionization equlibirium calculation were collisional ionization and radiative and dielectronic recombination. The recombination coefficients were taken from Aldrovandi and Pequignot (1973).

The essential features of Fig. 7 are that: a) ionization stages normally found in the upper and middle TR remain unaffected (see below). b) The temperature range over which lower ionization stages exist is generally broadened (on the low temperature side) and, in some instances, shifted to lower temperatures, and c) a density dependence is introduced into the ionization equilibrium.

Clearly, electron non-LTE effects significantly alter magnesium's ionization equilibrium. Qualitatively similar results have been found for C, N, O, Si, S, but it is felt premature to present extensive ionization equilibrium data until deficiencies in the present calculation are remedied. Four deficiencies in particular may alter the results shown in Fig. 7. First, the fact that the calculated temperature profile is too steep at low temperatures implies that ϕ^o departs from ϕ^* at lower values of ξ than is perhaps realistic. This leads to an overestimate of ionization rates for low ionization states. Second, ionization rates of higher ionization stages have been underestimated at low temperatures because in calculating the ionization rates I set ionization any rate for which $\xi_{1\kappa}$ exceeded 5.4 equal to zero. This turns out to be a poor approximation because the tail extends to many 10's of thermal velocities in the low TR. Third, I have not attempted to account for effects of the nonthermal electron energy spectrum on dielectronic recombination rates. However, because this process involves inelastic electron-ion collisions and, moreover, favors collisions with large excitation energy (e.g., Mihalas 1978), I suspect its rate will be significantly enhanced at temperatures below, say, 3×10^5 K. If it turns out that the rate of dielectronic recombination exceeds that of radiative recombination in the low TR, the ionization balance may be significantly different than shown in Fig. 7. Fourth, I note that provided the effect just mentioned does not qualitatively change present results, it is likely that at low temperatures the situation will be one in which neutral

hydrogen and helium coexist with multiply-charged trace elements. In this case charge transfer recombination of trace ions in collisions with atomic hydrogen and helium (Butler and Dalgarno 1980) may play an important role in the ionization balance.

From the above discussion it is apparent that a considerable amount of work remains to be done before reliable ionization equilibrium results are available.

Now consider the question of whether a non-thermal electron energy spectrum will cause enhanced emission in a given spectral line. Several cases can be distinguished. (i) If the fractional abundance curve of the relevant ion has not been broadened or shifted to lower temperature (e.g., Mg VI in Fig. 7), then enhanced emission is not expected. This is because an unaltered abundance curve implies $C_{1\kappa} \approx C^*_{1\kappa}$ over the temperature range in which the ion is abundant and, since $E_{12} < E_{1\kappa}$ and departures from a Maxwellian spectrum increase monotonically with energy, this implies $C_{12} \approx C^*_{12}$ over the same temperature range. (ii) If the ion's abundance curve has been shifted (e.g., Mg IV), and if E_{12} is comparable to $E_{1\kappa}$, then emission will be enhanced because a) emission occurs over a broader, more dense region than in LTE and b) because C_{12} is likely to exceed C^*_{12} over this range. Thus, resonance lines of hydrogen and helium (see below) are likely candidates to show enhanced emission. (iii) Finally, if the relevant abundance curve has been altered but E_{12} is small compared to $E_{1\kappa}$, then although enhanced emission will probably still occur due to density and range effects, the relative enhancement will be less than in case (ii) because C_{12} will be close to C^*_{12} over the region of formation.

The above remarks are clearly qualitative; detailed calculations are required if one is to draw reliable conclusions.

ii) Helium

The quiet sun XUV spectra of helium has evoked much interest in recent years (see Mango et al 1978 for a review), mainly because it is poorly understood. The central issue has been to identify the mechanisms responsible for ionizing HeI and HeII at low temperatures (Athay 1975, p. 298) and for enhancing resonance line intensities considerably in excess of that predicted by standard collisional excitation. Although it is now belived that a photoionization-radiative recombination mechanism is responsible for formation of the resonance continua of both HeI and HeII (Mango et al), the exciting mechanism for the HeI λ584 and HeII λ304 lines remains ambiguous. In 1975 Jordan suggested that what was needed was a method of mixing under-ionized helium with hotter electrons, thereby enhancing the line emission. Subsequently, Shine et al (1975) reported calculations which indicated diffusion of helium up the temperature gradient was one means of achieving such mixing. I show here that diffusion of fast electrons down the temperature gradient is a second.

In Table 7 I list ionization rate ratios, $C_{1\kappa}/C^{*}_{1\kappa}$, for HeI and HeII and excitation rate ratios for the HeI λ584 and HeII λ304 transitions. Both actual and LTE rates were calculated numerically using cross sections from Mihalas and Stone (1968). Note that the HeII rates are considerably enhanced even at 45,800 K, well above the temperature at which we expect thermalization to occur in a more realistic chromosphere model.

Proper assessment of how the collision rate enhancements indicated above affect helium's ionization balance and line emission requires radiative transfer calculations beyond the scope of this paper (see: Avrett et al 1976; Milkey et al 1973). The following qualitative observations may be noted however. First, it appears that helium's ionization balance will in fact be altered by the effects in question, for the enhanced collisional ionization

rates are comparable to the nominal photoionization rates for HeI and HeII quoted by Avrett et al. throughout the temperature range of interest. Second, the observed brightening of the helium resonance lines (and other EUV emission lines) in going from cell interior to network region can be understood, at least partially, in terms of the sun's large-scale magnetic field structure; i.e., the predominantly horizontal field in cell interiors impedes vertical diffusion of electrons. Third, the observed decrease in brightness of the helium resonance lines in coronal holes--which is more pronounced than for other ions (Jordan 1975, Bohlin 1977)--and their relative brightening in active regions can be understood in terms of i) their relatively large ratio of excitation to ionization energy, and ii) differences in physical conditions in these regions. i) implies the lines have large values of E_{12}/kT in their region of formation and hence are particularly sensitive to a non-thermal electron energy spectrum. Regarding ii) I note that a useful parameter for assessing the likelihood of non-Maxwellian effects is collisional depth τ_L separating high and low temperature regions. For an isobaric slab of thickness L, electron pressure P, maximum and minimum temperatures T_h and T_c, and possessing a conduction temperature profile (i.e., $T^{7/2}$ linear in height), I find that

$$\tau_L \equiv \int_0^L \frac{dz'}{\lambda(z')} \approx \frac{7L}{\lambda(T_h)} \approx \frac{7\pi e^4 \, P \, \ln\Lambda}{(kT_h)^3} \left(\frac{\langle \Delta \ln T \rangle}{L}\right)^{-1} ,$$

where I have assumed $T_h >> T_c$ so that $\langle \Delta \ln T \rangle \approx \frac{T_h - T_c}{T_h} \sim 1$. Coronal holes are thought to be cool, low-density regions with relatively weak temperature gradients, whereas active regions are hot, dense regions with steep gradients. Thus, τ_L most likely increases, and non-thermal effects therefore decrease, in going from active regions to holes. Fourth, and perhaps most interestingly, I note that in addition to its potential ability to account for the observed emission in the λ584 and λ304 resonance lines, the present theory helps explain a puzzling aspect of the helium spectrum, namely the large observed

values of the Lyman series intensity ratios for HeII; $I(n \rightarrow 1;\ n \geq 3)/I(2 \rightarrow 1)$. As noted by Zirin (1975), it is difficult to explain the observed intensity ratios via collisional excitation by electrons with a Maxwellian energy spectrum, because in this case the ratios scale $\exp(-\Delta E/kT)$, where ΔE is the difference in excitation energy and T is the (assumed common) temperature at which the lines are formed. On the other hand, photoionization of He II followed by recombination to excited states with subsequent radiative decay to ground gives line ratios in much better agreement with the data (Zirin). But excitation via this latter mechanism implies He II resonance lines are formed near optical depth unity in the He II continuumand hence at large line-center optical depths. If this were actually the case, however, the emergent line profiles should exhibit a central self-reversal (Milkey 1975), and they do not. Instead they are observed to be simple Gaussians, thereby indicating an excitation mechanism operative at small line-center optical depths.

The above dilemma can potentially be resolved by allowing for collisional excitation by electrons with an energy spectrum which is softer than exponential, such as those calculated here. It is hoped to pursue this and other aspects of the helium problem in a later publication.

V. Discussion

a) Implications for Transition-Region Physics

There are several outstanding questions concering the low TR ($T \lesssim 3 \times 10^5$ K), other than those related to the helium spectrum discussed in § IV, for which electron non-LTE effects hold implications. Among these are the following.

i) Energy Balance

Energy balance in the low TR is widely considered to be problematic (e.g., Athay 1981, Alvarez 1980, Pallavicini *et al.* 1981, Chiuderi and Riani 1974). Broadly stated, the problem is that empirical temperature profiles are inconsistent with known energy-transfer mechanisms, while temperature profiles derived from energy-balance arguments fail to reproduce the observations.

The shortcomings of classical conduction-radiation models are especially interesting because the empirically inferred conductive flux at the top of the quiet-Sun TR of approximately 5×10^5 ergs/cm^2-sec is sufficient to balance radiative losses from the transition region and upper chromosphere (Athay 1981). There are two difficulties. On the one hand, semi-empirical analysis of EUV line intensity data (e.g., Athay 1966, Dupree 1972, Kopp 1972; see also Withbroe 1977) suggests that transition-region temperature gradients are roughly consistent with constant conductive flux for 10^5 K $\lesssim T < 10^6$ K, but decrease sharply immediately below 10^5 K. Since the classical heat flux is proportional to $T^{5/2} \frac{dT}{dz}$, a decrease in $\frac{dT}{dz}$ implies a large conductive energy input to this material near 10^5 K. As recognized by Kuperus and Athay (1967) and others, however, plasma of solar composition at 10^5 K and transition-region pressures cannot

radiate sufficiently rapidly to dispose of the incoming energy, so that mass motion should result. Moreover, as a result of this energy deposition near 10^5 K, there is an insufficient conductive energy flux into the upper chromosphere, where the bulk of the radiative loss actually occurs. Thus, in order to reconcile the empirical temperature profile with energy balance one requires an energy sink near 10^5 K and an energy source at lower temperatures (Athay 1981).

On the other hand, although they permit conductive energy in amount sufficient to balance radiative losses to reach the upper chromosphere, (classical) conduction-radiation models also prove incompatible with energy balance. This is because at upper chromospheric temperatures the temperature gradient required to carry the conductive flux is so large (e.g., at 3×10^4 K, $\left(\frac{d\ell nT}{dz}\right)^{-1} \approx 0.1$ Km if $q_{cond} = 5 \times 10^5$ ergs/cm^2-sec) that there is insufficient material in the required temperature range to produce the observed radiation. This effect was encountered in § III of this paper, when establishing the reference temperature scale $T_o(z)$.

The above difficulties have led to consideration of alternatives to one-dimensional, static, conduction-radiation models. However, neither alteration of the geometry (Gabriel 1976), nor consideration of enthalpy transport by steady flows (Pneuman and Kopp 1978, Chiuderi and Riani 1974) have significantly changed the situation; to account for the observations one still requires an energy sink near 10^5 K and an energy source at lower temperatures.

Now consider the possibilities suggested by results reported here and by more recent calculations (Paper II). First, it is plausible that rise in the empirical differential emission measure near 10^5 K is due to electron non-LTE effects on ionization equilibria and line emission, as illustrated in Fig. 7 for magnesium and discussed in detail in § IV. Lines which in (electron) LTE are formed over a relatively narrow temperature range near 10^5 K are perhaps actually formed over a significantly broader, lower temperature, and hence higher density range, with correspondingly enhanced emission. If so, there need not be a sharp decline in the temperature gradient immediately below 10^5 K, thus obviating the need for an energy sink in this region. This view is supported by the observational evidence discussed below. Second, based on recent calculations using the Bhatnagar, Gross and Krook equation (Paper II), I suggest that the conductive energy flux into the upper chromosphere is carried by suprathermal electrons with velocities extending to 10-30 times local thermal velocities. Since energy deposition by suprathermal electrons is due primarily to Coulomb collisions with background electrons, energy deposition per unit pathlength is largely independent of the local temperature structure. Conductive energy transfer via this mechanism might therefore overcome the small scalelength problems inherent to classical conduction.

To summarize, I suggest that it may be possible to construct kinetic conduction-radiation models of the TR which are consistent with the observations and with energy balance. To do so requires that conduction and radiation be calculated, and observations interpreted, with proper allowance for electron non-LTE effects.

Within the context of this paper this is, of course, only a conjecture; detailed calculations are required in order to reach firm conclusions. Moreover, if this is to be the case, the role of energy transport by mass motion remains to be clarified (Athay and Holzer 1982). Nonetheless, the preliminary results reported here, the simplicity and economy of the underlying ideas and the observational evidence discussed below lend some weight to the stated conjectures.

ii) The Schmahl and Orrall (1979) Observation

The above authors have reported evidence for strong continuum absorption of EUV line photons with wavelengths shortward of 912 Å everywhere on the Sun's disk. The lines involved had $4.8 \leq \log T_{max} \leq 5.6$, where T_{max} is the temperature at which the standard line contribution function is maximum. As discussed by Schmahl and Orrall, two possible explanations are i) that due to the inhomogeneous nature of the atmosphere there is a large amount of cool, neutral-hydrogen-containing material overlying the EUV-emitting regions (most likely in their opinion), or ii) that there may be a significant amount of neutral hydrogen (and helium) distributed more or less uniformly with the EUV-emitting ions.

I note that provided the additional effects discussed in § IVd do not qualitatively change the ionization balance, the second of the above alternatives is what one would expect on the basis of the ideas discussed in this paper. Ionic stages which in electron LTE exist only at relatively high temperatures ($2\text{-}3 \times 10^5$ K), may actually have significant populations throughout the upper chromosphere where there is a non-negligible concentration of neutral hydrogen.

What speaks against this intepretation is that the absorption appears to be as pronounced in cell interiors as in network regions. However, the magnetic field configuration in both network and cell interior regions is perhaps too uncertain for this objection to be decisive.

iii) Temperature Plateaus

Empirical, one-dimensional models of the upper chromosphere require substantial amounts of material at temperatures near 20,000 K in order to account for the observed resonance line and continuum spectrum of hydrogen (Vernazza et al. 1976, 1980, Basri et al. 1979, Gouttebroze et al. 1979). Although the existence of such plateaus can plausibly be attributed to inhomogeneities in the solar atmosphere, within the context of one-dimensional models they are problematic in two respects (Avrett 1981). First, it is difficult, from an energy-balance standpoint, to identify processes responsible for their formation, and second, spectrum synthesis for elements other than hydrogen often require plateaus with disparate properties. For example, Lites et al. (1978) find that their best fit to center-to-limb measurements of C II resonance lines at 133.5 nm, as well as hydrogen Ly-α and Lyman continuum intensities requires a plateau at 16,500 K with about 25% more material than the one at 20,000 K required by Vernazza et al. (1976) based on hydrogen data alone (see Vernazza et al. 1981). Loulergue and Nussbaumer (1976) note that the observed λ977 and λ1176 emission from C III can be explained by a plateau at 30,000 K with an electron density $n = 10^{10}$ cm^{-3} and a thickness of 800 km along the line of sight. This is especially noteworthy in the present context because standard calculations (Jordan 1969) indicate that C III

has its maximum abundance near 60,000 K. Finally, Feldman, Doschek and Patterson (1976) find that λ1207 emission from Si III is compatible with a plateau at 36,000 K with thickness 840 km in cell boundary regions and 380 km in cell interiors.

I suggest that the plateaus just mentioned are perhaps artifacts of the LTE assumption; i.e., they are required in present empirical models in order to compensate for underestimating collisional excitation and ionization rates.

iv) Non-local Thermodynamics

It follows from results shown in § IV that the detailed shape of the electron distribution function in the low TR is dependent on the global temperature and density structure of the overlying atmosphere. An implication of this is that the ionization equilibrium of the elements, optically thin radiative losses and energy transport by thermal conduction acquire a dependence on the global structure of the upper TR and corona. This siutation is in sharp contrast to that which attains in electron-LTE, where each of the above processes is a function of the local thermodynamic variables and perhaps their gradients. Clearly, breakdown of the local Maxwellian approximation in the solar TR--and by implication in the transition regions of other stars--leads to a significant increase in the level of complexity required for successful spectroscopic diagnostic work or theoretical modeling.

If future calculations give fractional abundance curves similar to the preliminary results for magnesium shown in Fig. 7, two added complications which may then arise are the necessity of considering charge transfer recombination reactions in the ionization balance and finite

optical-depth effects in resonance lines which are optically thin according to standard ionization equilibrium calculations.

Finally, I note that because the calculated electron energy spectrum has a relatively weak temperature (spatial) dependence in the low TR (Fig. 3), ionization nonequilibrium effects due to flows through this region (Joselyn et al. 1978, Raymond and Dupree 1978) may be less significant than presently thought.

v) Other Effects

The most straightforward test of the ideas discussed here lies in comparison of predicted and observed EUV emission-line profiles and intensities. However, there are two additional effects associated with a nonthermal electron spectrum which may be observable.

As mentioned in § II, it is well known that electron distributions of the sort calculated here imply an enhanced level of electron density fluctuations at frequencies near the local plasma frequency. (If the electron temperature exceeds the ion temperature, ion density fluctuations will also be excited.) In addition to their ability to scatter fast electrons (Tidman and Eviatar 1965)--an effect which should be included in future calculations--Tidman and Dupree (1965) and others have shown that such density fluctuations also lead to a significant collective contribution to the bremsstrahlung emission at the local plasma frequency and its first harmonic. For the TR the relevant frequency range is roughly .1 to 10 GHz. I find that for a model atmosphere consisting in an isobaric, constant conductive flux TR ($10^4 \leq T \leq 2 \times 10^6$ K, $N_e T_e = 6 \times 10^{14}$ cm^{-3}, $q = 6 \times 10^5$ ergs cm^{-2} sec^{-1}), together with an isothermal, hydrostatic corona

($T_{cor} = 2 \times 10^6$ K), the optical depth is less than unity for frequencies $\nu \gtrsim$ 7 GHz and .3 GHz for ω_p and $2\text{-}\omega_p$ emission, respectively. Although these numbers are quite model dependent, they indicate that it may be possible to observe enhanced ω_p and $2\text{-}\omega_p$ radiation from the TR.

Henoux et al. (1982) have observed linear polarization in the chromospheric S I 1437A line during the soft x-ray phase of a flare. The measured direction of polarization suggests that collisional excitation by an anisotropic electron distribution, such as those expected in a plasma carrying a heat flux, is the mechanism responsible for producing the polarization. If higher temperature lines suitable for polarization measurements could be identified, and measurements made, they might provide a valuable constraint on future calculations of the electron distribution function.

b) Previous Work

Spicer (1978) has noted that the large heat flux inferred from empirical models of the solar TR imply a return current electric field which is of the order of the Dreicer field. He suggests that as a result there occurs a "boiling off" of electrons in the tail of the electron distribution and that these electrons represent a non-negligible fraction of the total energy input to the corona.

This idea is incorrect. Present results show that in a temperature gradient fast electrons diffuse down the gradient against the action of the electric field. Spicer's error lies in accepting conventional ideas concerning electron runaway in a homogeneous plasma immersed in a dc electric field (Dreicer 1959). Reference to Eq. 41 shows that, in an inhomogeneous plasma, gradient-related terms dominate

electric field terms by a factor of $(\frac{v}{v_{th}})^2$ in the kinetic equation. The latter are, therefore, unimportant at suprathermal velocities.

Pursuing ideas (Shoub 1976) made available to him, Roussel-Dupré (1980) has examined the effect of an electron distribution function possessing a nonthermal tail on heat conduction and on the ionization equilibrium of several elements. Because there is no physical basis for his choice of distribution function, however, meaningful conclusions cannot be drawn from his analysis.

Gurevich and Istomin (1979) have attempted a perturbation analysis of the linearized, high velocity form of the Fokker-Planck equation, treating $\alpha = \lambda \frac{d\ nT}{dz}\Big|_{max}$ as a small parameter. Because they resort to quite severe idealizations (e.g., infinitely steep temperature gradients), their results appear to be only of qualitative significance. Nevertheless, they do point out classical heat conduction results are likely to be invalid for quite small values of α.

c) Summary

In the foregoing I have shown that the fundamental assumption that in a weakly inhomogeneous plasma free electrons maintain nearly a local-Maxwellian velocity distribution function is invalid throughout the solar transition region and upper chromosphere. I have examined several implications of the breakdown of this assumption and have suggested that a number of outstanding puzzles related to the low transition region--including energy balance, the anomalous resonance line spectrum of He I and He II, the anomalous continuum absorption by neutral hydrogen and the seeming need for plateaus in empirical one-dimensional temperature profiles of the upper chromosphere--are potentially resolvable by abandoning the electron-LTE hypothesis. In addition, I have identified several phenomena--non-local

heat conduction, enhanced electron-ion excitation, ionization and dielectronic recombination rates, charge transfer recombination on neutral hydrogen and helium and possible plasma collective effects--which may play a role in future development of this subject. These advances were made possible by development of an effective numerical algorithm for solving kinetic equations of the Fokker-Planck type.

Acknowledgments

I wish to thank Dr. B. Goldstein for reading and commenting on an early version of this manuscript, Dr. S. Antiochos for his patient listening and advice, Dr. C. McKee for alerting me to the possible relevance of charge transfer reactions and Dr. J. C. Henoux for bringing his EUV line polarization measurements to my attention. Finally, I gratefully acknowledge the help given to me by the staff of the computing facility of the National Center for Atmospheric Research.

This work was supported in part by NASA grants NGL 05-020-272 and NAGW-92 and Office of Naval Research Contract N00014-75-C-0673.

References

Aldrovandi, S. M. W., and Pequignot, D. 1973, Astr. and Ap., 25, 137.

Allen, C. W. 1973, Astrophysical Quantities (London: University of London).

Alvarez, M. 1980, Ap. J., 240, 322.

Athay, R. G. 1966, Ap. J., 145, 784.

Athay, R. G. 1976, The Solar Chromosphere and Corona: Quiet Sun (Holland: Reidel, Dordrecht).

Athay, R. G. 1981, in The Sun as a Star, ed. S. Jordan, NASA SP-450.

Athay, R. G. and Holzer, T. E. 1982, Ap. J., 255, 743.

Avrett, E. H. 1981, in Solar Phenom. in Stars and Stellar Systems, ed. Bonnet, R. M. and Dupree, A. K. (Boston: D. Reidel Publ. Co.), p. 173.

Avrett, E. H., Vernazza, J. E., and Linsky, L. 1976, Ap. J. (Letters), 207, L199.

Baldwin, D. E. and Watson, C. J. H. 1977, Plasma Phys., 19, 517.

Basri, G. H., Linsky, J. L., Bartoe, J., Brueckner, G., and Van Hooser, M. E. 1979, Ap. J., 230, 924

Bernstein, I. B. 1969 in Adv. in Plasma Phys., ed. Simon, A. and Thompson, W. B., Vol. 3, p. 127.

Bhatnagar, P. L., Gross, E. P., and Krook, M. 1954, Phys. Rev., 94, 511.

Dahlin, J. D. 1977, in Coronal Holes and High Speed Wind Streams, ed. Zerker, J. (Boulder: Colorado Univ. Press).

Butler, S. E. and Dalgarno, A. 1980, Ap. J., 241, 838.

Carrier, G. F., and Pearson, E. C. 1976, Partial Differential Equations (New York: Academic Press).

Chiuderi, C., and Riani, I. 1974, Solar Phys, 34, 113.

Dreicer, H. 1959, Phys. Rev., 115, 238.

_____ 1960, Phys. Rev., 117, 329.

Dupree, A. K. 1972, Astrophys. J., 178, 527.

Feldman, U., Doschek, G. A., and Patterson, N. P. 1976, Ap. J., 209, 170.

Gabriel, A. H. 1976, Phil. Trans. Roy. Soc. London A, 281, 339.

Gouttebroze, P., and Leibacher, J. W. 1980, Ap. J., 238, 1134.

Grad, H. 1962, in Proc. 5th Int'l. Conf. on Ioniz. Phenom. in Gases (Amsterdam: (N. Holland Pub. Co.), p. 1630.

Gurevich, A. V., and Istomin, Ya., N. 1979, JETP, 50 (3), 470.

Henoux, J. C. Chambe, G., Semel, M., Woodgate, B., Shine, R., and Beckers, J. 1982, Proc. 24th COSPAR Meeting (Ottawa, Canada).

Jordan, C. 1975, M.N.R.A.S., 170, 429.

Jordan, C. 1969, M.N.R.A.S., 142, 501.

Joselyn, J. Holzer, T. E., and Munro, R. H. 1979, Ap. J. Suppl., 40, 793.

Kershaw, D. S. 1978, J. Comput. Phys., 26, 43.

Killeen, J., and Marx, K. D. 1970, Methods in Computational Physics, Vol. 9 (New York: Academic Press).

Kopp, R. A. 1972, Solar Phys., 27, 373.

Kuperus, M., Athay, R. G. 1967, Solar Phys., 1, 361.

Landau, L. 1936, Physik Z. Sowjetunion, 10, 154.

_____ 1949, Phys. Rev., 77, 567.

Lites, B. W., Shine, R. A., and Chipman, E. G. 1978, Ap. J., 222, 333.

Loulergue, M., and Nussbaumer, H. 1976, Astr. Ap., 51, 163.

Mango, S. A., Bohlin, J. W., Glackin, D. L., and Linsky, J. L. 1978, Ap. J., 220, 683.

Manteuffel, T. A. 1977, Numer. Math., 28, 307.

McWhirter, R. W. P., and Wilson, R. 1975, Astron. and Astrophys., 40, 63.

Mihalas, D. 1978, Stellar Atmospheres (San Francisco: W. H. Freeman and Co.), p. 134.

Mihalas, D., and Stone, M. E. 1968, Ap. J., 151, 293.

Milkey, R. W. 1975, Ap. J. (Letters), 199, L131.

Milkey, R. W., Heasley, J. N., and Beebe, H. A. 1973, Ap. J., 186, 1043.

Morse, P. M., and Feshbach, H. 1953, Methods of Theoretical Physics, Vol 1 (New York: McGraw Hill).

Pallavicini, R., Peres, G., Serio, S., Vaiana, G. S., Golub, L., and Rosner, R. 1981, Ap. J., 247, 692.

Pneuman, G. W., and Lopp, R. A. 1978, Solar Phys., 57, 49.

Raymond, J. C., and Dupree, A. K. 1978, Ap. J., 222, 379.

Resibois, P., and De Leener, J. 1977, Classical Kinetic Theory of Fluids (New York: Wiley & Sons, Inc.).

Richtmyer, R. D., and Morton, K. W. 1967, Difference Methods for Initial-Value Problems (2nd ed.; New York: Interscience).

Rosenbluth, M. N., MacDonald, W., and Judd, D. 1957, Phys. Rev., 107, 1.

Roussel-Dupre, R. 1980a, Solar Phys., 68, 243.

_____ 1980b, Solar Phys., 68, 265.

Schmahl, E. J., and Orrall, F. Q. 1979, Ap. J., 231, L41.

Shine, R., Gerola, H., and Linsky, J. L. 1975, Ap. J. (Letters), 202, L101.

Siambis, J. G., and Stitzer, S. N. 1974, Phys. Fluids, 17, 2192.

Shoub, E. C. 1976, Proposal to Computing Facility NCAR (Boulder, Colo.), unpubl.

_____ 1977, Ap. J. Suppl., 34, 259.

_____ 1981, Bull. Am. Phys. Soc., 26, 1057.

_____ 1983, in preparation.

Spicer, D. W. 1979, Solar Phys., 62, 269.

Spitzer, L., Jr. 1962, Physics of Fully Ionized Gases (New York: Wiley), p. 132.

Spitzer, L., and Härm, R., 1953, Phys. Rev., 89, 977.

Tidman, D. A., and Dupree, T. H. 1965, Phys. Fluids, 8, 1860.

Tidman, D. A., and Eviatar, A. 1965, Phys. Fluids, 8, 2059.

Van Der Vorst, H. A. 1981, J. Comput. Phys., 44, 1.

Vernazza, J. E., Avrett, E. H., and Loesser, R. 1973, Ap. J., 184, 605.

Vernazza, J. E., Avrett, E. H., and Loesser, R. 1981, Ap. J. Suppl., 45, 635.

Withbroe, G. L. 1977, Proc. OSO-8 Workshop, LASP (U. of Colorado).

Zirin, H. 1975, Ap. J. (Letters), 199, L63.

Table 1.

Empirically Derived, Homogeneous Quiet-Sun Transition Region Model[a]

z	$\log T_o$	n_o	$\frac{dT_o}{dz}$	λ	α	$\xi_c = \alpha^{\frac{1}{4}}$
Km	°K	cm^{-3}	°K/Km	Km		
2006	4.8	9.5(9)	4.3(3)	3.3(-2)	2.2(-3)	4.6
2011	5.0	6.0(9)	1.1(4)	1.2(-1)	1.3(-2)	2.9
2016	5.2	3.8(9)	1.1(4)	4.6(-1)	3.2(-2)	2.4
2031	5.4	2.4(9)	3.6(3)	1.7	2.4(-2)	2.5
2512	5.8	9.5(8)	1.1(2)	26.4	4.6(-3)	3.8

[a] A. K. Dupree (1972)

[b] NOTE - Numbers in parenthesis denote multiplicative powers of 10.

Table 2a.

First Two Angular Moments of the Distribution Function for Three Coefficient Iterations for the Case $P = P_o$ at a Location Where

$\tau_1 = 27$, $T_o = 19{,}900K$, $\alpha = 3.8 \times 10^{-2}$

Iteration No. / ξ	$\phi^o(\xi, \tau_1)/\phi^*(\xi)$ [a]			$\phi^1(\xi, \tau_1)/\phi^*(\xi)$ [b]		
	1	2	3	1	2	3
0.5	1.00	.992	.985	7.35 (-3)	1.09 (-2)	1.30 (-2)
1.0	1.00	1.00	1.00	2.31 (-2)	3.50 (-2)	4.24 (-2)
1.5	.999	1.00	1.01	2.56 (-2)	4.00 (-2)	5.18 (-2)
2.0	.975	.973	.978	-4.13 (-2)	3.73 (-2)	-2.36 (-2)
2.5	.986	.988	.988	-3.02 (-2)	-3.15 (-2)	-3.01 (-2)
3.0	1.73	1.79	1.78	-1.13	-1.18	-1.16
4.0	1.08 (2)	1.15 (2)	1.13 (2)	-8.94 (1)	-9.43 (1)	-9.25 (1)
5.0	1.40 (5)	1.47 (5)	1.44 (5)	-1.21 (5)	-1.27 (5)	-1.25 (5)

[a] $\phi^o \equiv 1/2 \int_{-1}^{1} \phi(\mu, \xi, \tau_1)\, d\mu$; $\phi^1 \equiv 3/2 \int_{-1}^{1} \mu\, \phi(\mu, \xi, \tau_1)\, d\mu$

[b] First iterate corresponds to MFPA.

Table 2b.

Calculated Dimensionless Heat Flux for Three Coefficient Iterations At Same Location as in Table 2a

Iteration[a]	$q^{b,c}$
1	-1.04(-1)
2	-9.46(-2)
3	-7.47(-2)

[a] First iterate corresponds to MFPA.

[b] $q \equiv \int_{-1}^{1} \mu \, d\mu \int_{0}^{\infty} \xi^5 \, \phi(\mu, \xi, \tau_1)$

[c] Spitzer-Härm value for q is -8.06(-2)

Table 3.

Portion of Calculated Transition Region Model. $\langle n_o T_o \rangle = 6 \times 10^{-14}$ K cm^{-3}

Height cm	τ	T_o ^oK	λ cm	α	$\frac{d \log_{10} T_o}{dz}$ cm^{-1}	Q_{rad}[a] erg/(cm^3-sec)	q_{SH}[b] erg/(cm^2-sec)
0.0	0.0	8.1 (3)	9.7	2.3 (-2)	2.4 (-3)	2.1 (2)	-2.01 (5)
2.1 (2)	1.4 (1)	1.1 (4)	2.4 (1)	4.1 (-2)	1.7 (-3)	8.4 (0)	-4.20 (5)
1.1 (3)	2.8 (1)	2.0 (4)	1.2 (2)	3.7 (-2)	3.1 (-4)	1.7 (-1)	-5.12 (5)
4.6 (3)	4.1 (1)	3.2 (4)	4.5 (2)	3.0 (-2)	6.6 (-5)	2.9 (-2)	-5.12 (5)
1.6 (4)	5.5 (1)	4.6 (4)	1.3 (3)	2.5 (-2)	1.9 (-5)	1.4 (-2)	-5.12 (5)
4.6 (4)	6.9 (1)	6.3 (4)	3.2 (3)	2.1 (-2)	6.6 (-6)	1.7 (-2)	-5.13 (5)
1.7 (5)	9.0 (1)	9.3 (4)	1.0 (4)	1.7 (-2)	1.7 (-6)	9.8 (-3)	-5.14 (5)
3.8 (5)	1.0 (2)	1.2 (5)	1.9 (4)	1.6 (-2)	8.1 (-7)	6.1 (-3)	-5.16 (5)
1.0 (6)	1.2 (2)	1.6 (5)	4.5 (4)	1.4 (-2)	3.0 (-7)	3.4 (-3)	-5.18 (5)
4.1 (6)	1.6 (2)	2.4 (5)	1.5 (5)	1.1 (-2)	7.3 (-8)	1.4 (-3)	-5.24 (5)
1.7 (7)	2.0 (2)	3.6 (5)	5.0 (5)	9.1 (-3)	1.8 (-8)	3.7 (-4)	-5.33 (5)
1.4 (8)	2.8 (2)	6.9 (5)	3.3 (6)	6.8 (-3)	2.1 (-9)	4.7 (-5)	-5.45 (5)
1.6 (9)	4.1 (2)	1.5 (6)	2.6 (7)	4.9 (-3)	1.9 (-10)	8.9 (-6)	-5.69 (5)
5.9 (9)	4.8 (2)	2.0 (6)	7.1 (7)	4.3 (-3)	6.9 (-11)	2.6 (-6)	-5.83 (5)

[a] Q_{rad} is the radiative loss per unit volume

[b] q_{SH} is the Spitzer-Härm heat flux.

Table 4.

Kinetic Theory Values of Reduced Thermodynamic Variables

T_o(°K)	n/n_o	T/T_o	$\langle \xi_z \rangle$	$P_{\|\|}/P_\perp$	T_o(°K)	n/n_o	T/T_o	$\langle \xi_z \rangle$	$P_{\|\|}/P_\perp$
		$P = P_o$					$P = P_o/2$		
1.12(4)	1.011	1.008	-0.002	1.016	1.12(4)	1.020	1.026	0.004	1.027
3.15(4)	1.006	0.999	-0.002	1.006	3.23(4)	1.012	1.007	-0.002	1.015
6.27(4)	1.004	0.999	-0.002	1.003	6.55(4)	1.009	1.002	-0.003	1.010
1.17(5)	1.003	0.999	-0.001	1.003	1.10(5)	1.007	1.000	-0.002	1.007
2.39(5)	1.002	0.998	-0.001	1.003	2.35(5)	1.005	0.999	-0.002	1.004
6.93(5)	1.001	0.999	-0.001	1.001	6.90(5)	1.003	0.998	-0.001	1.002

Table 5.

Normalized Isotropic Component of Distribution Function
$\phi^{\circ}(\xi,T_o)/\phi^{*}(\xi)$

ξ	$T_o = 1.5 \times 10^4$K		$T_o = 3.1 \times 10^4$K		$T_o = 1.57 \times 10^5$K		$T_o = 6.92 \times 10^5$K	
	P_o	$P_o/2$	P_o	$P_o/2$	P_o	$P_o/2$	P_o	$P_o/2$
0.00	0.99	0.98	0.99	0.98	1.00	1.00	1.00	1.00
0.28	0.99	0.98	1.00	0.98	1.00	1.00	1.00	1.00
0.57	0.99	0.99	1.00	0.99	1.00	1.00	1.00	1.00
0.85	1.00	1.00	1.00	1.00	1.00	1.00	1.00	1.00
1.13	1.00	1.00	1.00	1.00	1.00	1.00	1.00	1.00
1.41	1.00	1.00	1.00	1.00	1.00	1.00	1.00	1.00
1.70	0.99	0.98	1.00	0.98	1.00	1.00	1.00	1.00
1.98	0.98	0.94	0.99	0.94	1.00	0.98	1.00	1.00
2.26	0.97	0.92	0.98	0.92	1.00	0.97	1.00	0.99
2.54	1.02	1.08	1.00	1.08	1.00	0.99	1.00	0.99
2.82	1.3	1.8	1.2	1.8	1.03	1.2	1.01	1.03
3.10	2.4	4.1	1.8	4.1	1.21	1.8	1.04	1.2
3.39	6.1	1.5(1)	4.0	1.3(1)	1.8	3.9	1.2	1.8
3.67	2.1(1)	6.1(1)	1.2(1)	3.4(1)	3.74	1.2(1)	1.6	3.9
3.95	9.3(1)	3.2(2)	5.0(1)	1.6(2)	1.1(1)	4.9(1)	3.1	1.1(1)
4.24	5.2(2)	2.0(3)	2.6(1)	9.5(2)	4.5(1)	2.5(2)	8.0	4.4(1)
4.52	3.6(3)	1.6(4)	1.7(3)	6.9(3)	2.4(2)	1.6(3)	2.9(1)	2.2(2)
4.80	3.0(4)	1.5(5)	1.4(4)	6.1(4)	1.6(3)	1.3(4)	1.4(2)	1.3(3)
5.08	3.1(5)	1.6(6)	1.3(5)	6.5(5)	1.4(4)	1.3(5)	8.8(2)	9.8(3)
5.36	3.8(6)	2.2(7)	1.6(6)	8.3(6)	1.5(5)	1.6(6)	6.8(3)	8.2(4)
5.65	5.7(7)	3.5(8)	2.3(7)	1.3(8)	1.9(6)	2.2(7)	6.3(4)	7.8(5)
5.93	1.0(9)	4.6(9)	3.9(8)	2.3(9)	3.0(7)	3.8(8)	6.3(5)	8.2(6)

Table 6.

Ratio of Calculated to Maxwellian Collisional-Ionization Rates for Mg.

T_e(°K)	Mg I			Mg II			Mg III			Mg IV			Mg V			Mg VI		
	$C_{1\kappa}/C^*_{1\kappa}$			$C_{1\kappa}/C^*_{1\kappa}$			$C_{1\kappa}/C^*_{1\kappa}$			$C_{1\kappa}/C^*_{1\kappa}$			$C_{1\kappa}/C^*_{1\kappa}$			$C_{1\kappa}/C^*_{1\kappa}$		
	$\xi_{1\kappa}$[a]	P_o	$P_o/2$	$\xi_{1\kappa}$	P_o	$P_o/2$	$\xi_{1\kappa}$	P_o	$P_o/2$	$\xi_{1\kappa}$	P_1	$P_o/2$	$\xi_{1\kappa}$	P_o	$P_o/2$	$\xi_{1\kappa}$	P_{o1}	$P_o/2$
11,200	2.8	7.5	1.9 (1)	3.9	2.2 (3)	7.7 (3)	9.1	-	-	1.1 (1)	-	-	1.2 (1)	-	-	1.4 (1)	-	-
20,000	2.1	1.2	1.6	3.0	7.6	2.0 (1)	6.8	-	-	7.8	-	-	9.1	-	-	1.0 (1)	-	-
32,300	1.7	1.0	1.1	2.3	1.4	2.0	5.4	3.6 (7)	1.2 (8)	6.3	-	-	7.2	-	-	8.2	-	-
47,500	1.4	1.0	1.0	1.9	1.0	1.1	4.4	2.1 (4)	6.8 (4)	5.2	6.2 (6)	1.9 (7)	5.9	-	-	7.4	-	-
65,500	1.2	1.0	1.0	1.6	1.0	1.0	3.8	1.9 (2)	6.1 (2)	4.4	1.3 (4)	4.1 (4)	5.0	1.5 (6)	4.3 (6)	5.8	2.5 (8)	2.1 (9)
86,500	1.0	1.0	1.0	1.4	1.0	1.0	3.3	1.1 (1)	3.2 (1)	3.8	2.1 (2)	6.6 (2)	4.4	7.6 (3)	2.4 (4)	5.0	9.4 (5)	2.8 (6)
110,300	9.0 (-1)	1.0	1.0	1.3	1.0	1.0	2.9	2.5	5.4	3.4	1.5 (1)	4.4 (1)	3.9	2.0 (2)	6.5 (2)	4.4	8.7 (3)	2.8 (4)
166,900	7.3 (-1)	1.0	1.0	1.0	1.0	1.0	2.4	1.1	1.3	2.6	1.6	2.6	3.0	3.9	5.3	3.4	2.7 (1)	3.5 (1)
235,100	6.1 (-1)	1.0	1.0	8.6 (-1)	1.0	1.0	2.0	1.0	1.0	2.3	1.1	1.2	2.7	1.3	1.8	3.0	2.2	4.8
315,300	5.3 (-1)	1.0	1.0	7.4 (-1)	1.0	1.0	1.7	1.0	1.0	2.0	1.0	1.0	2.3	1.0	1.1	2.6	1.2	1.5

[a] $\xi_{1\kappa}$ = electron threshold velocity/local thermal velocity

Table 7.

Ratio of Calculated to Maxwellian Collision Rates For Helium

	$\frac{C_{1\kappa}(HeI)}{C^*_{1\kappa}}$		$\frac{C_{1\kappa}(HeII)}{C^*_{1\kappa}}$		$\frac{C_{12}(\lambda 584)}{C^*_{12}}$		$\frac{C_{12}(\lambda 304)}{C^*_{12}}$	
	P_o	$P_o/2$	P_o	$P_o/2$	P_o	$P_o/2$	P_o	$P_o/2$
1,200	3.8(6)	1.5(7)	-	-	1.3(6)	5.2(6)	-	-
5,000	1.4(4)	5.7(4)	-	-	8.4(3)	3.6(4)	3.1(8)	1.6(9)
9,900	2.2(2)	7.4(2)	2.5(8)	1.1(9)	2.0(2)	6.7(2)	5.7(5)	2.2(6)
5,400	1.8(1)	4.9(1)	1.4(6)	5.0(6)	1.8(1)	5.3(1)	6.1(3)	2.0(4)
1,500	3.9	8.8	2.1(4)	6.6(4)	4.3	1.0(1)	2.6(2)	7.8(2)
8,300	1.7	3.0	8.7(2)	2.7(3)	1.9	3.5	2.9(1)	8.0(2)
5,800	1.2	1.6	8.5(1)	2.5(2)	1.3	1.8	6.5	1.6(1)
3,900	1.1	1.2	1.6(1)	4.3(1)	1.1	1.3	2.6	5.1
2,700	1.0	1.1	5.0	1.2(1)	1.1	1.2	1.5	2.4
2,100	1.0	1.1	2.4	4.6	1.0	1.1	1.2	1.6
2,300	1.0	1.0	1.5	2.4	1.0	1.0	1.1	1.2
3,100	1.0	1.0	1.2	1.6	1.0	1.0	1.0	1.1
4,600	1.0	1.0	1.1	1.3	1.0	1.0	1.0	1.1

Figure Captions

Figure 1. A plot of the pitch angle dependence of the reduced distribution function at a fixed velocity and location, illustrating the convergence properties of the iterative scheme discussed in the text. Curves are labeled by iteration number. Thus, curve "0" is the initial estimate, curve "1" is the result of the first forward ($\mu>0$) integration, curve "2" is the result of the first backward ($\mu<0$) integration, etc.

Figure 2. Isotropic part of the reduced distribution function versus dimensionless energy at several heights for $P = P_0$. Abscissa; $\xi^2 = \frac{mv^2}{2kT_0(z)}$. Ordinate; $\phi^\circ(\xi, T_0) = 1/2 \int_{-1}^{1} \phi(\mu, \xi, T_0)\, d\mu$. Solid lines are calculated results. Dashed line is a local Maxwellian. Solid curves are labeled with the value of T_0 at the corresponding height.

Figure 3. Isotropic part of the dimensional distribution function versus velocity measured in units of 10^8 cm/sec for the case $P = P_{0/2}$. Dashed lines are local-Maxwellian distributions; solid lines are calculated results.

Figure 4. One-dimensional reduced distribution function of electron velocities along the gradient direction at several heights, including upper and lower boundaries. ξ_z is positive in the direction of increasing temperature. Solid lines represent calculated results. Dashed lines are local Maxwellians.

Figure 5. Normalized pitch angle dependence of the distribution function for a sequence of velocities at a location near the bottom of the slab ($T_0 = 47{,}500$K). μ is the positive in the direction of increasing temperature. Note ordinate scale changes between panels.

Figure 6. Contour plot of the reduced distribution function for $P = P_0$ and at the same location as in Fig. 5. ξ_z is the component of the dimensionless velocity along the gradient direction and is positive in the direction of increasing temperature.

Figure 7. Normalized pitch angle dependence of the distribution function at the lower boundary. The boundary condition is $\phi(\mu, \xi, \tau = 0) = \phi^*(\xi)$ for $\mu > 0$.

Figure 8. Fractional relative abundance of the first six ionization stages of magnesium versus temperature for $P = P_0$ and $P_0/2$. Solid lines are for calculated collision rates. Dashed lines are for Maxwellian rates.

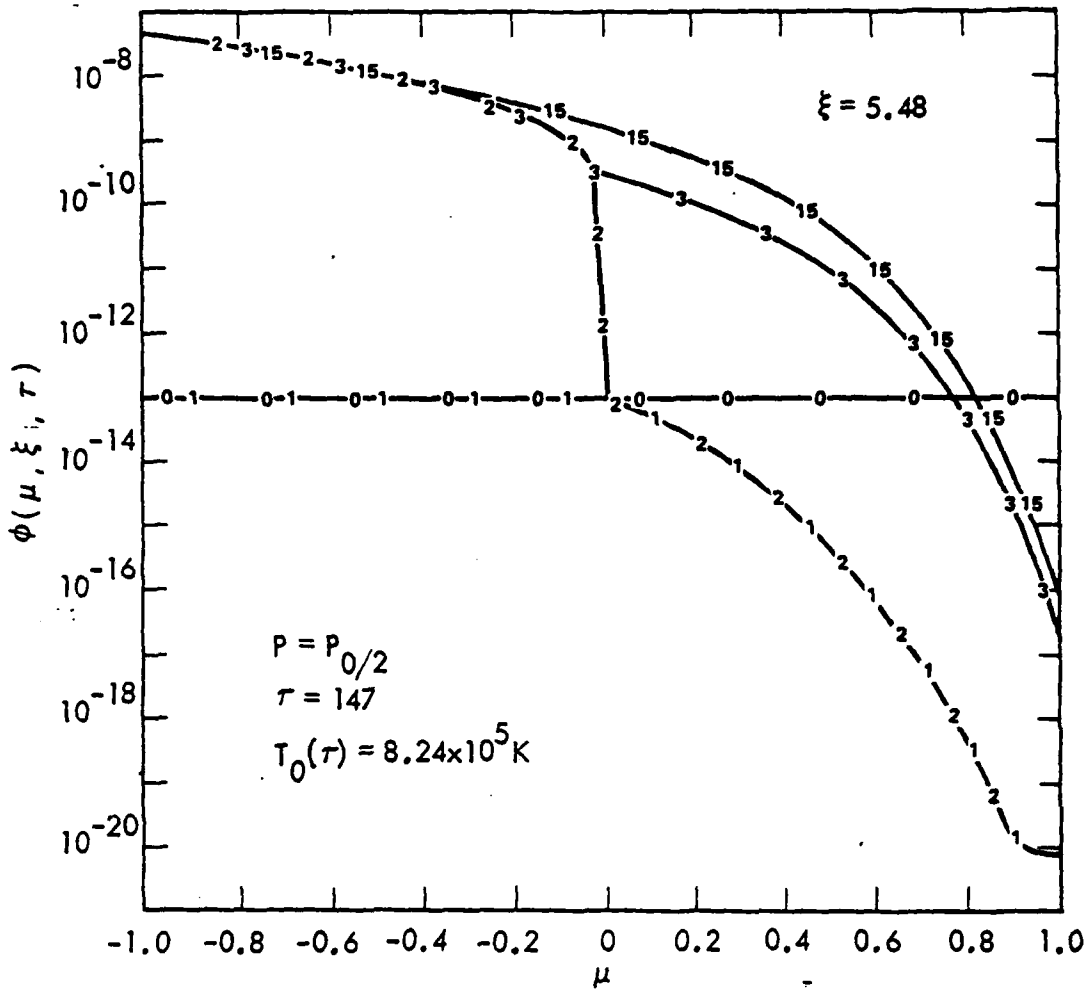
$\xi = 5.48$
$P = P_{0/2}$
$\tau = 147$
$T_0(\tau) = 8.24 \times 10^5 K$
$\phi(\mu, \xi, \tau)$
μ
10^{-8}
10^{-10}
10^{-12}
10^{-14}
10^{-16}
10^{-18}
10^{-20}
-1.0 -0.8 -0.6 -0.4 -0.2 0 0.2 0.4 0.6 0.8 1.0

Figure 1

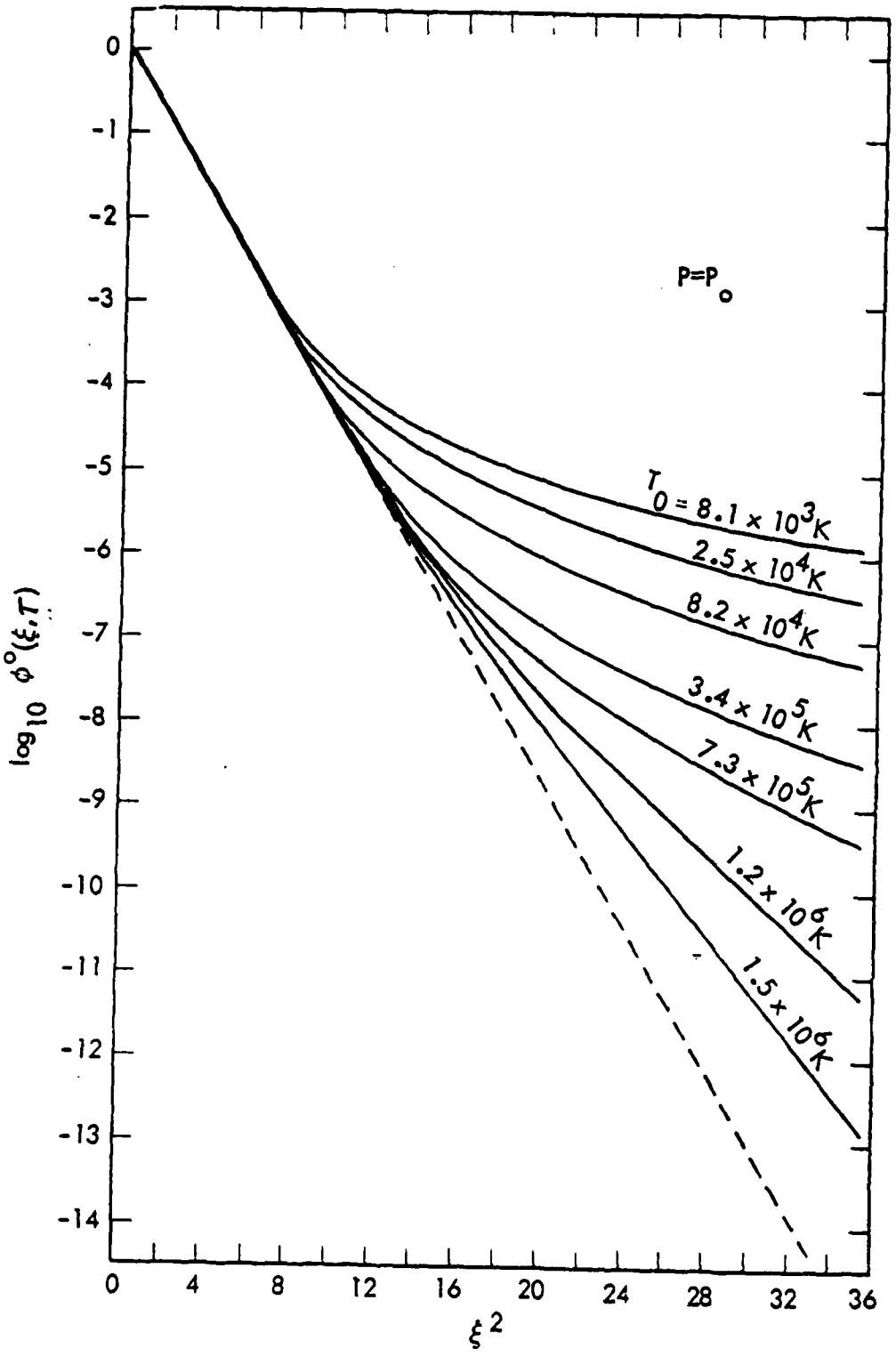
0
-1
-2
-3
-4
-5
-6
-7
-8
-9
-10
-11
-12
-13
-14
$\log_{10} \phi^{\circ}(\xi, T)$
P=P$_o$
$T_0 = 8.1 \times 10^3$K
2.5×10^4K
8.2×10^4K
3.4×10^5K
7.3×10^5K
1.2×10^6K
1.5×10^6K
0
4
8
12
16
20
24
28
32
36
ξ^2

Figure 2

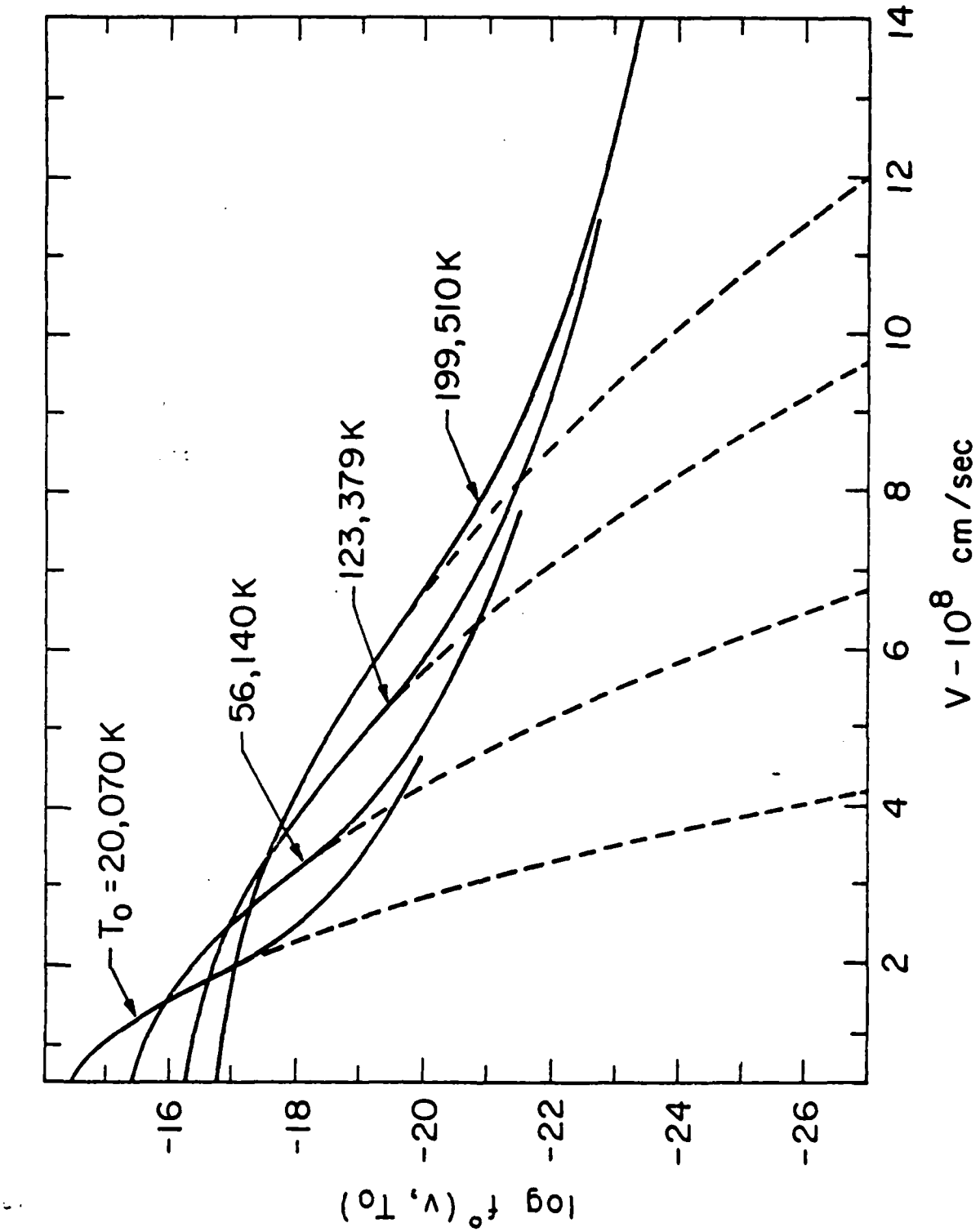
$T_0 = 20,070\,K$
56,140 K
123,379 K
199,510 K
log $f^0(v, T_0)$
-16
-18
-20
-22
-24
-26
2
4
6
8
10
12
14
$V - 10^8$ cm/sec

Figure 3

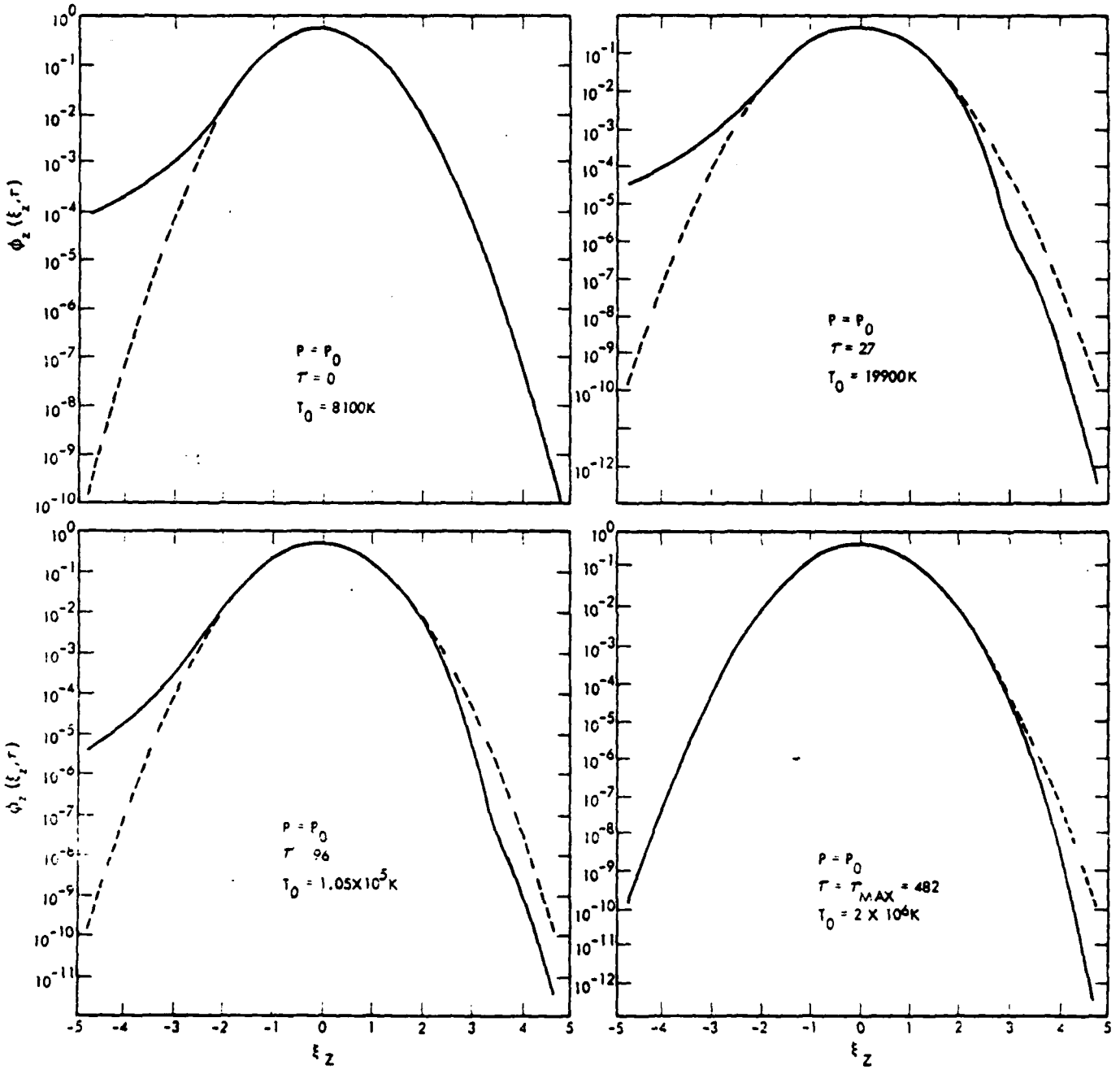
$\Phi_z(\xi_z, \tau)$
$P = P_0$
$\tau = 0$
$T_0 = 8100K$
$P = P_0$
$\tau = 27$
$T_0 = 19900K$
$P = P_0$
$\tau = 96$
$T_0 = 1.05 \times 10^5 K$
$P = P_0$
$\tau = \tau_{MAX} = 482$
$T_0 = 2 \times 10^6 K$
ξ_z

Figure 4

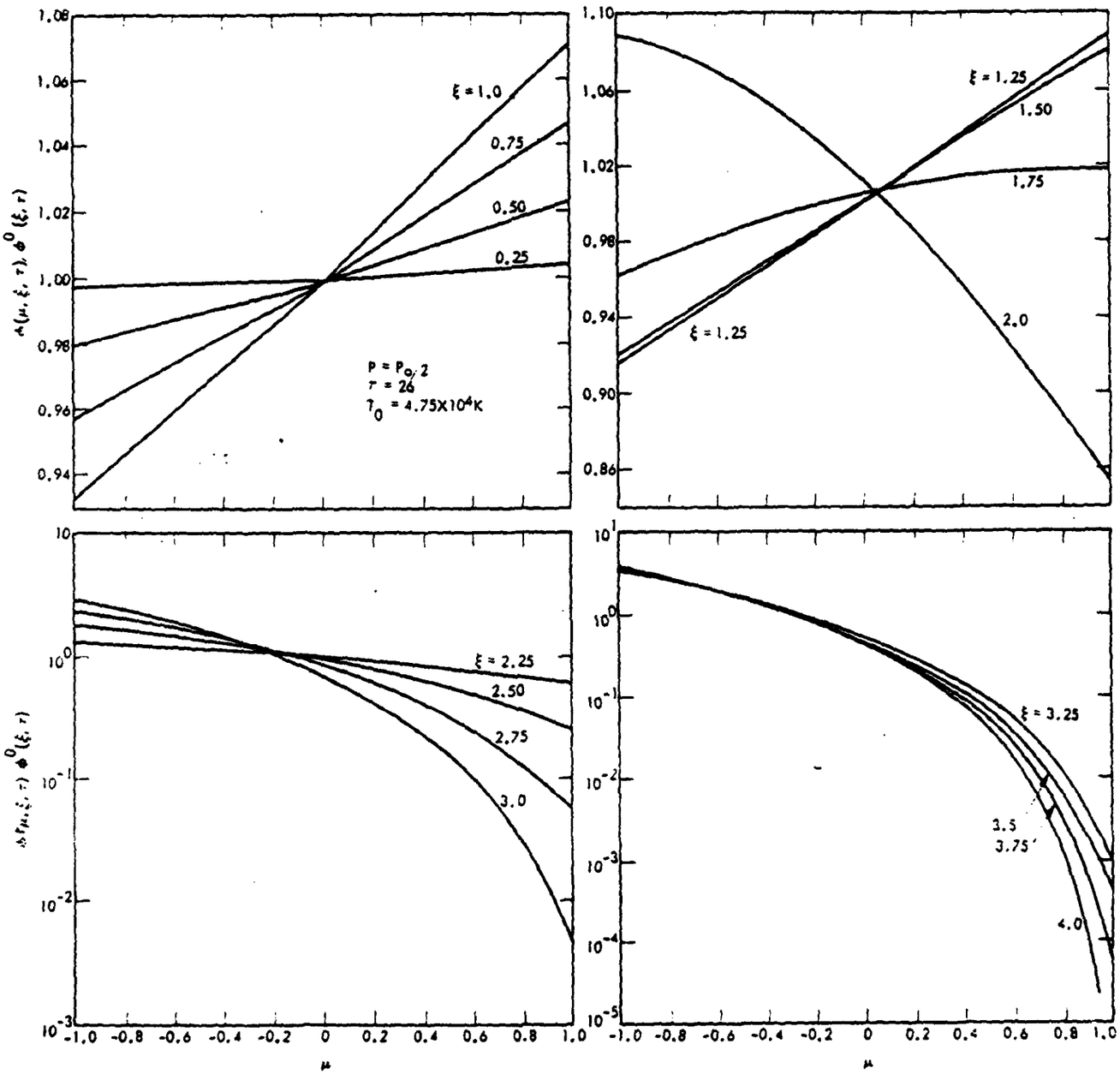
ξ = 1.0
0.75
0.50
0.25
P = P0/2
τ = 2δ
T0 = 4.75X10⁴K
ξ = 1.25
1.50
1.75
2.0
ξ = 2.25
2.50
2.75
3.0
ξ = 3.25
3.5
3.75
4.0
μ
μ

Figure 5

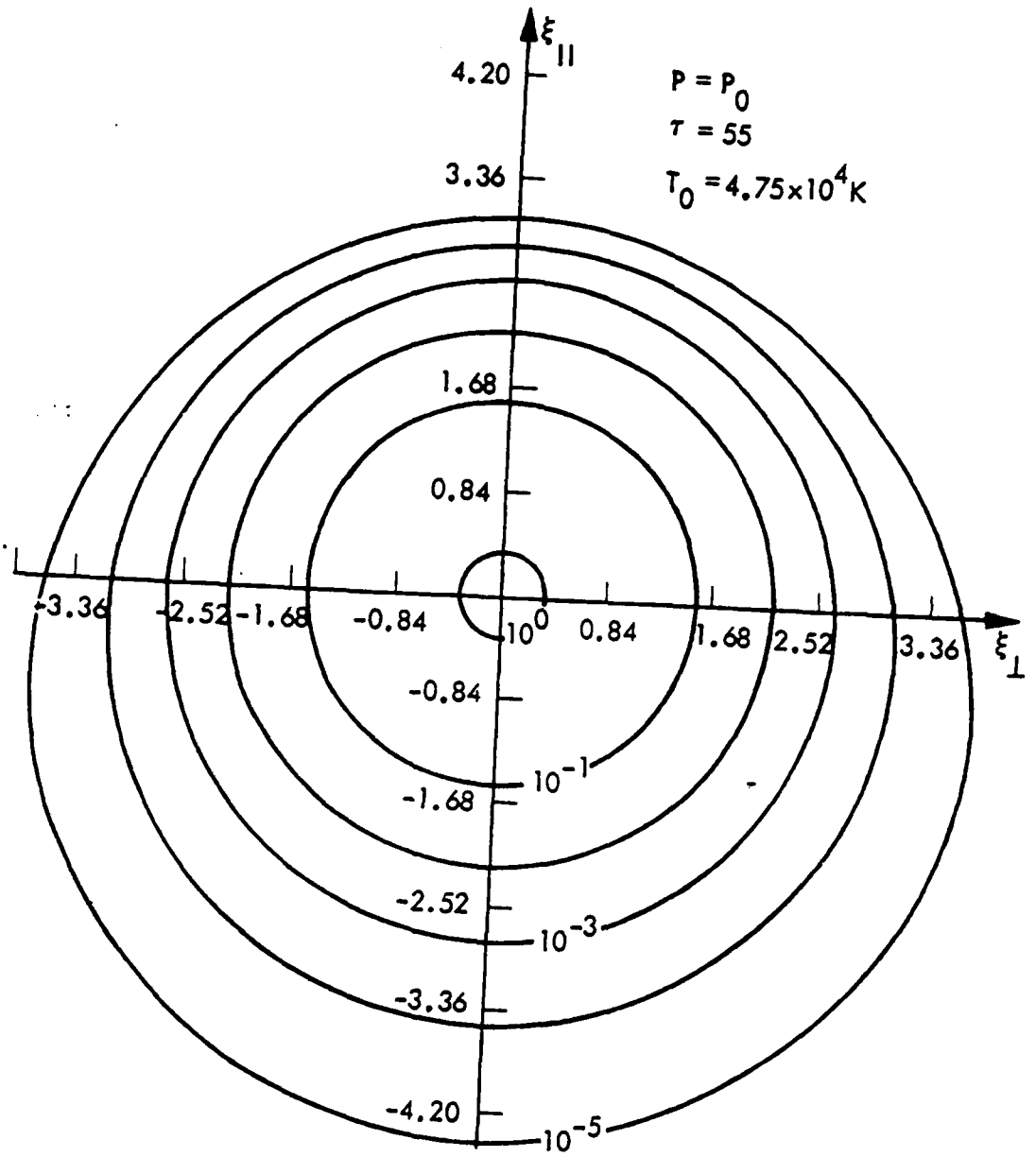
ξ_{11}
4.20
3.36
1.68
0.84
-0.84
-1.68
-2.52
-3.36
-4.20
P = P0
τ = 55
T0 = 4.75×10^4K
-3.36
-2.52
-1.68
-0.84
10^0
0.84
1.68
2.52
3.36
$\xi_{\perp}$
10^-1
10^-3
10^-5

Figure 6

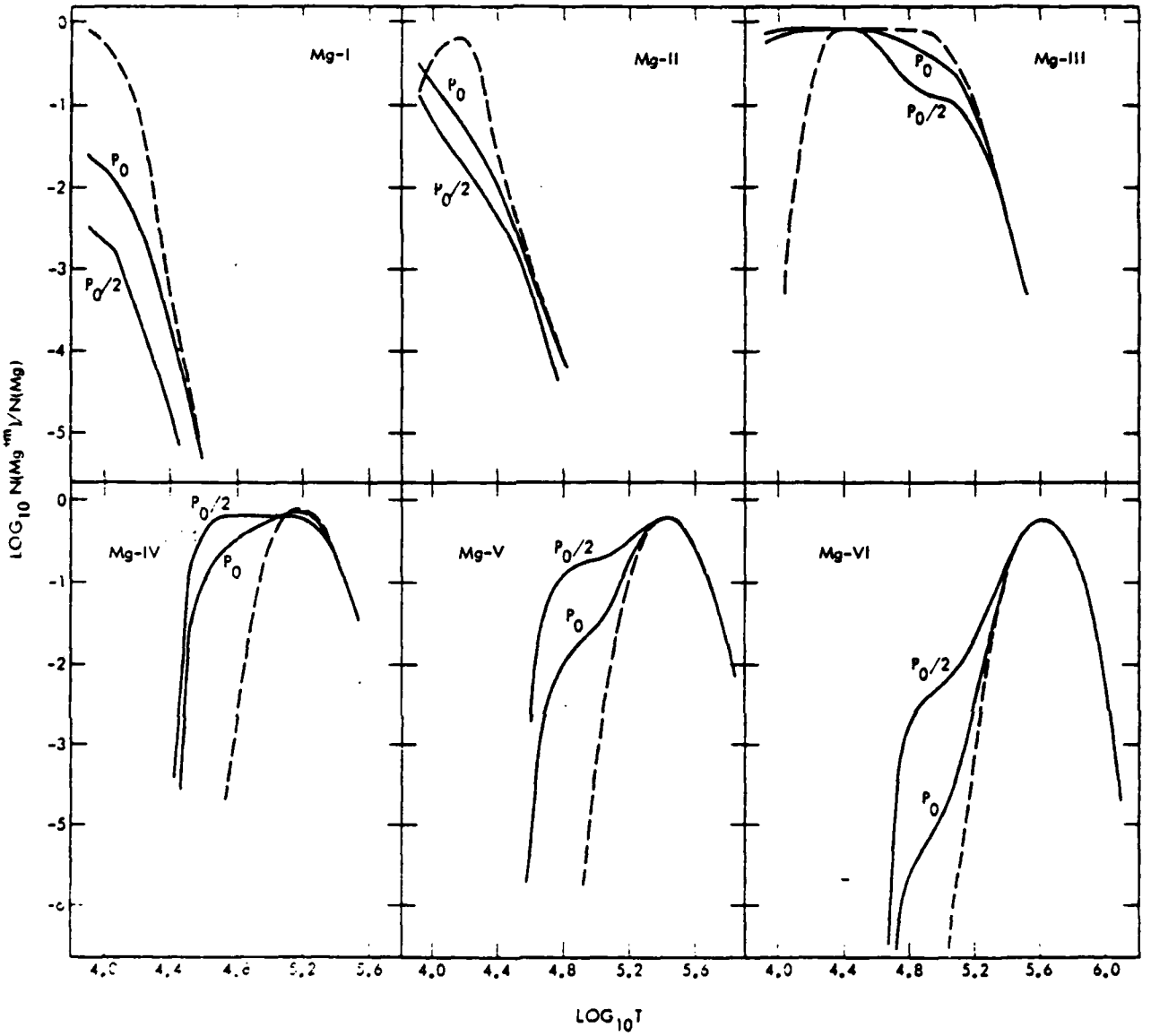

Figure 7

Appendix

Here I give heuristic arguments supporting the step-size estimates (49a,b).

Consider first the case of explicit differencing. In their book Richtmyer and Morton (1968, p. 207) use a standard Von Neumann stability analysis to show, under the condition that the coefficients be slowly varying, that if Eq. (47) is differenced using a forward (explicit) time difference and centered, second-order space differences, the stability condition is

$$\Delta t \left(\frac{A'}{(\Delta x)^2} + \frac{C'}{(\Delta y^2)} \right) \leq \frac{1}{2} \tag{A1}$$

This is a local condition in that it must be satisfied for all x, y in the region of interest.

Disregarding the fact that the coefficients in Eq. 45 are not slowly varying, the analogous condition for stability of an explicit differencing scheme for that equation (using centered second-order μ and ξ-differences) is

$$\Delta\tau \left(\frac{A}{(\Delta\xi)^2} + \frac{C}{(\Delta\mu)^2} \right) \leq \frac{1}{2} \tag{A2}$$

From Eq. (43) we see that in the MFPA, $A \to \frac{2}{3\sqrt{\pi}}$ and $C \to \xi^{-3}$ as $\xi \to 0$. Since the smallest values of μ and ξ on the mesh are $\frac{\Delta\mu}{2}$ and $\Delta\xi$, (A2) implies

$$\Delta\tau \leq 0 \left\{ (\Delta\mu) \quad (\Delta\xi)^2 \right\} \tag{A3}$$

which is (49a) of the text. Due to the rapid variation of the coefficients, (A3) is most probably incorrect as a rigorous stability criterion. Nevertheless,

it is probably not very wrong and thus indicates that the singular nature of the coefficients in the Fokker-Planck equation near $\xi = 0$ leads to excessively small step sized restrictions for explicit spatial differencing schemes.

Now consider application of ADI-differencing (Richtmyer and Morton, p. 211) to Eq. (48b) in the MFPA, so that by (39b) the mixed-derivative term is absent. In this case (48b) can be written

$$\frac{\partial \underline{\phi}^+}{\partial \tau} = (\underline{\underline{L}}_\xi + \underline{\underline{L}}_\mu)\, \underline{\phi}^+(\tau) + \underline{q}\,(\tau) \tag{A4}$$

where for $\xi \neq 0$, ξ_{max}, $\underline{\underline{L}}_\xi$ and $\underline{\underline{L}}_\mu$ are difference-matrix representations of the operators $\frac{1}{\mu\xi}\left\{a^*\partial^2_{\xi\xi} + \left[d^* + \mu\left(\frac{\alpha\xi^2}{2} - \beta\right)\right]\partial_\xi + P^* + \frac{5}{2}\alpha\mu\xi\right\}$ and $\frac{1}{\mu\xi}\left\{c^*\,\partial_{\mu\mu} + \left[e^* + \frac{(1-\mu^2)}{\xi}\,\beta\right]\partial_\mu\right\}$ respectively. The vector $\underline{q}$ denotes the term $\underline{\underline{N}}^+\,\underline{\phi}^-$ in (48b) and is considered known. Elements of $\underline{\underline{L}}_\mu$ and $\underline{\underline{L}}_\xi$ for $\xi = 0, \xi_{max}$ correspond to the difference form of the side conditions (44) and (42) respectively. Using the notation $\underline{\phi}^i = \phi(i\Delta\tau)$ and omitting the + superscript from $\underline{\phi}^+$, the ADI scheme for (A4) may be written

$$\begin{aligned}
\frac{\underline{\phi}^{i+1/2} - \underline{\phi}^i}{\Delta\tau/2} &= \underline{\underline{L}}_\xi\, \underline{\phi}^{i+1/2} + \underline{\underline{L}}_\mu\, \underline{\phi}^i + \underline{q}^i \\
\frac{\underline{\phi}^{i+1} - \underline{\phi}^{i+1/2}}{\Delta\tau/2} &= \underline{\underline{L}}_\xi\, \underline{\phi}^{i+1/2} + \underline{\underline{L}}_\mu\, \underline{\phi}^{i+1} + \underline{q}^{i+1}
\end{aligned} \tag{A5}$$

Upon eliminating $\underline{\phi}^{i+1/2}$ I find that

$$\begin{aligned}
\frac{\underline{\phi}^{i+1} - \underline{\phi}^i}{\Delta\tau} = \frac{1}{2}(\underline{\underline{L}}_\xi + \underline{\underline{L}}_\mu)\left\{\underline{\phi}^i + \underline{\phi}^{i+1}\right\} + \frac{1}{2}\left\{\underline{q}^i + \underline{q}^{i+1}\right\} \\
- \frac{(\Delta\tau)^2}{4}\left\{\underline{\underline{L}}_\xi\, \underline{\underline{L}}_\mu \frac{(\underline{\phi}^{i+1} - \underline{\phi}^i)}{\Delta\tau} + \underline{\underline{L}}_\xi \frac{(\underline{q}^{i+1} - \underline{q}^i)}{\Delta\tau}\right\}
\end{aligned} \tag{A6}$$

I observe that the first two bracketed terms on the right side of (A6) are the result for a fully implicit (hereafter FI) step, centered at i + 1/2. The last term on the right in (A6) is thus $\left.\frac{\partial \phi}{\partial \tau}\right|_{ADI} - \left.\frac{\partial \phi}{\partial \tau}\right|_{FI}$. In usual applications of the ADI method (slowly varying coefficients) this difference is of order $(\Delta\tau)^2$, and is acceptably small because the truncation error of the FI step is itself of order $(\Delta\tau)^2$. In our case, however, this term is large at small velocities.

To see this we make use of the fact that for conditions of interest the computed solution is close to the (1953) Spitzer-Härm solution at small velocities; i.e.,

$$\phi\ (\mu,\xi,\tau) \approx \phi^*\ (\xi) + 2\mu\ \alpha\ (\tau)\ \phi^1\ (\xi)$$

where

$$\phi^1\ (\xi) = \left\{ D_T\ (\xi) - 0.35\ D_E\ (\xi) \right\} \phi^*$$

and D_T and D_E are the functions tabulated by Spitzer & Härm. I find that $\phi^1\ (\xi) = 0\ (\xi^{4+\delta})$ as $\xi \to 0$ where $0<\delta<<1$. Using the definitions given above for the operators L_μ and L_ξ I now find that

$$L_\xi\ L_\mu \left(\frac{\phi^{i+1} - \phi^i}{\Delta\tau} \right) \xi \to 0\ 0 \left[\frac{d\alpha}{d\tau} \frac{1}{\mu \xi^{3-\delta}} \right] \qquad \text{(A7)}$$

Since $\frac{d\alpha}{d\tau} = 0(\alpha^2)$, the requirement that $\left| \frac{\partial \phi}{\partial \tau}_{ADI} - \frac{\partial \phi}{\partial \tau}_{FI} \right| << \phi$ for all μ,ξ leads, with help of (A6) and (A7), to the condition that

$$\alpha \Delta\tau \leq 0 \left[\Delta\ \mu\ (\Delta\xi)^3 \right]^{1/2}$$

which is (49b) of the text.

Edward C. Shoub

Institute for Plasma Physics

Stanford University

Stanford, California 94305

END

FILMED

12-82

DTIC